Physics of Fluids

Instability induced by wall deformability in sliding Couette flow

Ramkarn Patne[1] and V. Shankar[1, a)]
Department of Chemical Engineering, Indian Institute of Technology, Kanpur 208016, India

The linear stability of 'sliding Couette flow' of a Newtonian fluid through the annular gap formed by two concentric cylinders having a ratio of inner to outer cylinder radii, β, and driven by the axial motion of the inner cylinder, is studied in the low Reynolds number (< 1) regime. The inner wall of the outer cylinder is lined by a deformable neo-Hookean solid layer of dimensionless thickness H. This flow configuration is encountered in medical procedures such as thread-injection and angioplasty, where the inserted needle is surrounded by the deformable wall of blood vessels. In stark contrast to the configuration with rigid cylinders, we predict the existence of finite- and short-wave linear instabilities even in the creeping-flow limit, driven by the deformable nature of the outer cylinder. Interestingly, these instabilities exist for arbitrary β, and even for non-axisymmetric perturbations, in parameter regimes where the flow is stable for the configuration with rigid outer cylinder. For the finite-wave instability, the axisymmetric mode is the most critical mode of the instability while the non-axisymmetric mode with azimuthal wavenumber $n = 4$ is the critical mode for the short-wave instability. By replacing the outer rigid boundary surrounding the deformable wall by an 'unrestrained' stress-free boundary, we demonstrate that the flow becomes significantly more unstable. Thus, the present study shows that the sliding Couette flow with a deformable wall can be linearly unstable at arbitrarily low Reynolds number, in direct contrast to the stability of the same configuration with a rigid cylinder.

[a)]Author for correspondence; E-mail: vshankar@iitk.ac.in

I. INTRODUCTION

Sliding Couette flow, also referred to as thread annular flow, consists of a fluid between the annular gap formed by two concentric cylinders of different radii, and is driven by the relative motion of the inner cylinder in the axial direction, as shown schematically in figure 1. This flow configuration is encountered in industrial processes such as wire coating[1], pipe linings[2] and manufacturing of optical fibers[3]. Recently, there is renewed interest in studying the stability of this flow due to its relevance to medical procedures such as thread injection[4–7] and angioplasty[8]. These studies, however, assumed the outer cylindrical boundary to be a rigid-walled cylinder. However, in the biological context, the deformable nature of the vessel wall can play an important role in introducing qualitatively new instabilities. With this motivation, the present work presents a comprehensive account of the stability of sliding Couette flow with a deformable outer boundary.

For the case of rigid outer cylinder, the linear stability of sliding Couette flow was first studied by Preziosi and Rosso[9], who predicted the flow to be linearly stable. Later, Gittler[10] predicted the existence of the instability when the inner cylinder to outer cylinder radii ratio is less than 0.1415 at Reynolds number (Re) of $O(10^6)$ for axisymmetric disturbances. Walton[4–6], motivated by applications in the thread-injection procedure, studied both linear and non-linear stability of annular Poiseuille-Couette flow. These studies confirmed the existence of a linear instability for axisymmetric disturbances predicted by Gittler[10]. Further, their analyses predicted non-axisymmetric modes to be more unstable than axisymmetric disturbances in the non-linear regime for the annular Poiseuille-Couette flow. However, linear and non-linear stability analysis of sliding Couette flow by Deguchi and Nagata[7] predicted axisymmetric disturbances to be most unstable mode. In order to understand the role of the transient growth of the disturbances in the destabilization of the flow, Liu and Liu[11] carried out a non-modal stability analysis of sliding Couette flow. Their analysis predicted non-modal growth of disturbances at Reynolds numbers lower than that predicted by the linear stability analysis and it was shown to be present even when the inner cylinder to outer cylinder radii ratio is greater than 0.1415.

Previous studies related to the stability of sliding Couette flow have hitherto considered rigid-walled cylinders[5–7,9–12]. However, in the case of the medical applications such as angioplasty, this analysis clearly needs to be generalized to account for the deformable walls present in blood vessels. It is now well established that deformable walls can introduce instabilities even in the creeping-flow limit[13,14]. Additionally, in industrial processes such as wire coating and manufacturing of optical fibers, the instabilities in the flow needs to be controlled, as such instabilities may result in unintended manufacturing defects in the finished product. In such cases, a deformable wall can be introduced in order to manipulate the instabilities[15]. Previous studies on plane Couette flow past a deformable surface in the creeping-flow limit predict two classes of the instabilities, viz., finite-wave and short-wave modes[13,14,16]. The finite-wave instability is characterized by a critical wavenumber (k_c) < 1 and dimensionless top-plate velocity (Γ_c) < 2 in the present non-dimensionalization scheme as explained in Sec III. This instability is driven by the shear work done by the fluid on the deformable surface at the fluid-deformable solid interface. The short-wave instability has its origin in the discontinuity of the non-zero first normal stress difference across the fluid-deformable-solid interface. The short-wave instability is predicted when neo-Hookean[14] or Mooney-Rivlin[17] models are used for the deformable solid, since these models predict non-zero first normal stress difference. The short-wave instability is characterized by $k_c > 1$ and $\Gamma_c > 2$ in the present non-dimensionalization scheme. In stark contrast to the instability of plane Couette flow past a deformable wall even in the creeping-flow limit, pressure-driven flows in channel and pipe configurations with a deformable wall are stable in the same limit[16,17]. Recent work in the

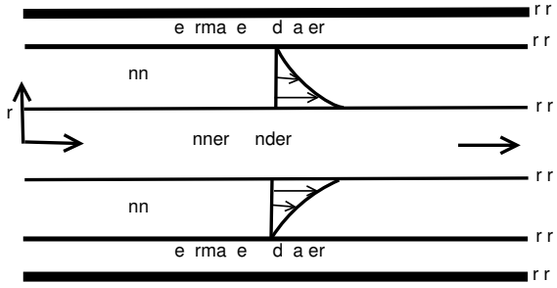

FIG. 1. Side view schematic of the flow geometry. The inner cylinder moves at a steady dimensionless speed Γ. The fluid is present in the annular gap $r_i \leq r \leq r_o$ while deformable solid is present in $r_o \leq r \leq r_o + H$. At $r = r_o + H$, deformable solid is perfectly bonded to a rigid solid.

area of flow past deformable solid surfaces has examined different facets of instabilities including in stratified flow[18] in deformable channels, non-Newtonian flows[19,20], resonant unstable modes in viscoelastic fluids[21], and finally the role of an unrestrained deformable boundary in inducing new modes of instability[22].

Despite the presence of deformable walls in the medical procedures as described above, its role on the stability of the sliding Couette configuration has not been examined in the existing literature. The objective of this work is, therefore, to provide a comprehensive understanding of the role of wall deformability on sliding Couette flow, by extending the aforementioned earlier efforts pertaining to rigid walls to a configuration with deformable walls. In this regard, we consider two different configurations: in the first configuration, the annular gap is surrounded by a deformable wall, which itself is rigidly bonded to an outer cylinder. This is the configuration that has been extensively studied in the previous literature[23]. While this configuration might be relevant to laboratory experiments[24], in the biological context, the deformable vessel walls are 'unrestrained', not being rigidly bonded to an outer cylinder. While the former configuration with a rigid outer cylinder allows for a rigorous mathematical formulation, the latter unrestrained configuration does not allow for the same. However, by using stress-free boundary conditions to mimic the unrestrained boundary, the qualitative effects of an unrestrained boundary on the stability of sliding Couette flow can be understood well. Following the earlier work of Refs. 14 and 16, we use the neo-Hookean constitutive relation to model the deformation in the wall for the case where the deformable wall is rigidly bonded to the outer cylinder. For the unrestrained case, we use a simplistic linear elastic model for the deformable wall. We show that, despite the cylindrical configuration involved, the sliding Couette flow with a deformable wall is predicted to become unstable even in the creeping-flow limit, in stark contrast to pressure-driven flow in a deformable tube[16]. We further show that the unrestrained nature of the boundary can make the flow significantly more unstable compared to the rigidly bonded configuration. The rest of the paper is organized as follows. The base state and linearized perturbed state equations are derived in Sec. II. The results obtained are presented and discussed in Sec. III. The salient conclusions of the present work are presented in Sec. IV.

II. PROBLEM FORMULATION

We consider a Newtonian fluid of density ρ^* and viscosity μ^* flowing through the annular gap between two cylinders, where the superscript $*$ denotes a dimensional quantity. The inner cylinder

is of radius r_i^* and moves with steady velocity V^* relative to the stationary outer cylinder of inner radius r_o^*. The inner wall of the outer cylinder is lined with a neo-Hookean solid of shear modulus G^* and thickness HR^*. The schematic of the flow geometry under consideration in terms of the dimensionless variables is shown in figure 1. Following the earlier studies of Deguchi and Nagata[7] and Liu and Liu[11], we non-dimensionlize lengths by $R^* = (r_o^* - r_i^*)/2$, velocities by V^*, pressure and stresses by $\mu^* V^*/R^*$. The velocity field in the fluid is given by $\mathbf{v} = (v_r, v_\theta, v_z)$ with v_r, v_θ and v_z being the components in the r, θ and z directions, respectively. The dimensionless governing equations for the fluid are

$$\nabla \cdot \mathbf{v} = 0, \tag{1}$$

$$Re\left(\frac{\partial \mathbf{v}}{\partial t} + (\mathbf{v}\cdot\nabla)\,\mathbf{v}\right) = -\nabla p + \nabla^2 \mathbf{v}, \tag{2}$$

where $Re = \rho^* V^* R^*/\mu^*$ is the Reynolds number. We denote $\beta = r_i^*/r_o^*$ such that dimensionless radii of the inner and outer cylinders are respectively $r_i = 2\beta/(1-\beta)$ and $r_o = 2/(1-\beta)$. The boundary conditions applicable to the configuration are as follows. At $r = r_i$, no-slip boundary condition implies $\bar{v}_z = 1$, where overbar implies a base-state quantity. Since the deformable solid is perfectly bonded to the rigid solid at $r = r_o + H$, it can only deform but will not move with the solid, thus assumption of no-slip implies $\bar{v}_z = 0$ at $r = r_o$. To obtain the base state, we assume steady, fully-developed flow

$$\bar{v}_z = \frac{\log\left(r(1-\beta)/2\right)}{\log(\beta)} \tag{3}$$

The overbar on v_z in the above equation and henceforth indicates base state quantity unless otherwise stated.

For the deformable wall, we use the neo-Hookean model and Lagrangian-three-state (L3) formulation for the deformable solid proposed by Patne *et al.*[25] to formulate the coupled problem. The L3 formulation essentially involves treating the solid in a Lagrangian framework, while the fluid is treated in the Eulerian framework with consistent base-state and interface conditions[25]. Let us consider a representative solid particle having coordinates $\mathbf{X} = (R, \Theta, Z)$ in the undeformed base state. The material point in the solid undergoes displacement due to the fluid flow past it, thus its position vector is $\bar{\mathbf{x}} = (\bar{r}, \bar{\theta}, \bar{z})$. The deformed and undeformed state coordinates of the representative solid particle are related by $\bar{\mathbf{x}}(\mathbf{X}) = \mathbf{X} + \bar{\mathbf{u}}_{\mathbf{x}}(\mathbf{X})$ where $\bar{\mathbf{u}}_{\mathbf{x}}(\mathbf{X})$ is the displacement vector. The inner cylinder moves in the z direction and we assume negligible displacement in the radial and azimuthal directions. The assumption is reasonable because of the absence of the pressure gradient in the base flow and incompressibility of the solid. Thus, for fully developed flow $\bar{\mathbf{u}}_{\mathbf{x}}(\mathbf{X}) = (0, 0, \bar{u}_z(R))$. The incompressibility condition is given by $\det(\bar{\mathbf{F}}) = 1$ where $\bar{\mathbf{F}} = \frac{\partial \bar{\mathbf{x}}}{\partial \mathbf{X}}$ is the base state deformation gradient. Using the non-dimensionalization scheme described above, the base state Cauchy stress tensor $\bar{\boldsymbol{\sigma}}$ and momentum equation for the solid are

$$\bar{\boldsymbol{\sigma}} = -\bar{p}_s \mathbf{I} + \frac{1}{\Gamma}\,\bar{\mathbf{F}}\cdot\bar{\mathbf{F}}^T, \tag{4}$$

$$\nabla_{\mathbf{X}} \cdot \bar{\mathbf{P}} = 0. \tag{5}$$

Here, $\bar{\mathbf{P}} = \bar{\mathbf{F}}^{-1}\cdot\bar{\boldsymbol{\sigma}}$ is the base state first Piola-Kirchoff stress tensor and $\bar{p}_s$ is the base state pressure in the solid. The above equations are to be solved by using following boundary conditions. At the fluid-deformable-solid interface ($r = r_o$), normal stress continuity implies constant pressure field in the deformable solid while tangential stress continuity gives the deformation gradient. At $r = r_o + H$, since deformable solid is perfectly bonded to a rigid solid, thus $\bar{u}_z = 0$. Following

the procedure developed by Patne *et al.*[25], the base state deformation of the solid in terms of the deformed state coordinates is

$$\bar{u}_z = \Gamma \frac{\log\left(\bar{r}/(r_o + H)\right)}{\log(\beta)}. \tag{6}$$

Here, $\Gamma = \mu^* V^*/(G^* R^*)$ is the dimensionless velocity of the inner cylinder. The parameter Γ can also be interpreted as ratio of the viscous stress in the fluid to the elastic stress in the deformable solid.

On the above base state, we impose infinitesimally small axisymmetric and non-axisymmetric perturbations. In the case of deformable wall, we track the representative particle in the perturbed state which has position vector $\mathbf{x}(\bar{x}) = \bar{\mathbf{x}} + \mathbf{u}'(\bar{x})$ where prime over any quantity signifies a perturbed state quantity and $\mathbf{u}'(\bar{x})$ is the perturbed state displacement of the particle. The deformation gradient to map the particle position from the deformed base state to the perturbed state is $\mathbf{F}' = \frac{\partial \mathbf{x}}{\partial \bar{\mathbf{x}}}$. Thus, the total deformation gradient, $\mathbf{F}$ to map the particle position from the undeformed base state to the perturbed state is

$$\mathbf{F} = \frac{\partial \mathbf{x}}{\partial \mathbf{X}} = \frac{\partial \mathbf{x}}{\partial \bar{\mathbf{x}}} \cdot \frac{\partial \bar{\mathbf{x}}}{\partial \mathbf{X}} = \mathbf{F}' \cdot \bar{\mathbf{F}}. \tag{7}$$

By using the deformation gradients defined above, the governing equations for the deformable wall in the perturbed state are

$$\det\left(\mathbf{F}'\right) = 1, \tag{8}$$

$$\boldsymbol{\sigma} = -p_s \mathbf{I} + \frac{1}{\Gamma}\, \mathbf{F} \cdot \mathbf{F}^T, \tag{9}$$

$$Re \frac{\partial^2 \mathbf{u}}{\partial t^2} = \nabla_{\bar{\mathbf{x}}} \cdot \mathbf{P}. \tag{10}$$

Here, $\mathbf{P} = (\mathbf{F}'^{-1} \cdot \boldsymbol{\sigma})$ and $\boldsymbol{\sigma}$ are respectively the perturbed state first Piola-Kirchoff stress tensor and Cauchy stress tensor. After linearising the above governing equations about the base state, we substitute normal modes of the following form

$$(v_r', v_\theta', v_z', p')(r, \theta, z) = (\tilde{v}_r, \tilde{v}_\theta, \tilde{v}_z, \tilde{p})(r) e^{(ikz + in\theta - ikct)}, \tag{11}$$

$$(u_r', u_\theta', u_z', p_s')(\bar{r}, \bar{\theta}, \bar{z}) = (\tilde{u}_r, \tilde{u}_\theta, \tilde{u}_z, \tilde{p}_s)(\bar{r}) e^{(ik\bar{z} + in\bar{\theta} - ikct)}, \tag{12}$$

where over-tilde indicates eigenfunction of the corresponding quantity. After using the normal modes, the linearised perturbed state governing equations for the fluid become

$$D\tilde{v}_r + \frac{\tilde{v}_r}{r} + \frac{in}{r}\tilde{v}_\theta + ik\tilde{v}_z = 0, \tag{13}$$

$$-D\tilde{p} + \left(D^2 + \frac{1}{r}\,D - \frac{1+n^2}{r^2} - k^2\right)\tilde{v}_r - \frac{2in}{r^2}\tilde{v}_\theta = Re[ik\tilde{v}_r(\bar{v}_z - c)], \tag{14}$$

$$-\frac{in}{r}\tilde{p} + \left(D^2 + \frac{1}{r}\,D - \frac{1+n^2}{r^2} - k^2\right)\tilde{v}_\theta + \frac{2in}{r^2}\tilde{v}_r = Re[ik\tilde{v}_\theta(\bar{v}_z - c)], \tag{15}$$

$$-i\,k\,\tilde{p} + \left(D^2 + \frac{1}{r}\,D - \frac{n^2}{r^2} - k^2\right)\tilde{v}_z = Re[ik\tilde{v}_z(\bar{v}_z - c) + D\bar{v}_z\tilde{v}_r], \tag{16}$$

where $D = d/dr$. Similarly, for the deformable solid, the linearised perturbed state governing equations become

$$D\tilde{u}_r + \frac{\tilde{u}_r}{r} + \frac{in}{r}\tilde{u}_\theta + ik\tilde{u}_z = 0, \quad (17)$$

$$\left(D^2 + \frac{1}{r}D + 2ikD\bar{u}_z D - \frac{1+n^2}{r^2} + \frac{ik}{r}D\bar{u}_z + ikD^2\bar{u}_z - k^2 - k^2(D\bar{u}_z)^2\right)\tilde{u}_r - \frac{2in}{r^2}\tilde{u}_\theta - \Gamma D\tilde{p}_s = -k^2c^2Re\Gamma\tilde{u}_r, \quad (18)$$

$$\left(D^2 + \frac{1}{r}D + 2ikD\bar{u}_z D - \frac{1+n^2}{r^2} + \frac{ik}{r}D\bar{u}_z + ikD^2\bar{u}_z - k^2 - k^2(D\bar{u}_z)^2\right)\tilde{u}_\theta + \frac{2in}{r^2}\tilde{u}_r - \frac{in\Gamma}{r}\tilde{p}_s = -k^2c^2Re\Gamma\tilde{u}_\theta, \quad (19)$$

$$\left(D^2 + \frac{1}{r}D + 2ikD\bar{u}_z D - \frac{n^2}{r^2} + \frac{ik}{r}D\bar{u}_z + ikD^2\bar{u}_z - k^2 - k^2(D\bar{u}_z)^2\right)\tilde{u}_z - ik\Gamma\tilde{p}_s = -k^2c^2Re\Gamma\tilde{u}_z, \quad (20)$$

where $D = d/d\bar{r}$. The above governing equations are to be solved by using the following boundary conditions. At $r = r_i$, rigid boundary is present, thus no-slip and impermeability of the fluid at the inner cylinder surface implies

$$\tilde{v}_r = 0; \quad \tilde{v}_\theta = 0; \quad \tilde{v}_z = 0. \quad (21)$$

At $r = r_o$, the continuity of the velocity and stresses at the fluid-deformable-solid interface gives

$$\tilde{v}_r = -ikc\tilde{u}_r, \quad (22)$$

$$\tilde{v}_\theta = -ikc\tilde{u}_\theta, \quad (23)$$

$$\tilde{v}_z + (D\bar{v}_z)_{r=r_o}\tilde{u}_r = -ikc\tilde{u}_z, \quad (24)$$

$$D\tilde{v}_z + ik\tilde{v}_r + (D^2\bar{v}_z)_{r=r_o}\tilde{u}_r = \frac{1}{\Gamma}\left(ik(D\bar{u}_z)_{r=r_o} + D\right)\tilde{u}_z + \frac{1}{\Gamma}\left(ik + (D\bar{u}_z)_{r=r_o}D\right)\tilde{u}_r, \quad (25)$$

$$\left(D - \frac{1}{r_o}\right)\tilde{v}_\theta + \frac{in}{r_o}\tilde{v}_r = \frac{1}{\Gamma}\left(D - \frac{1}{r_o} + ik(D\bar{u}_z)_{r=r_o}\right)\tilde{u}_\theta + \frac{in}{\Gamma r_o}\tilde{u}_r, \quad (26)$$

$$-\tilde{p} + 2D\tilde{v}_r = -\tilde{p}_s + \frac{1}{\Gamma}\left(2D + 2ik(D\bar{u}_z)_{r=r_o}\right)\tilde{u}_r - \frac{T}{\Gamma}(1-k^2)\tilde{u}_r. \quad (27)$$

Here, $()_{r=r_o}$ signifies evaluation of the base state quantities at $r = r_o$. The parameter, $T = T^*/(GR)$ is the dimensionless interface tension with T^* as the dimensional interface tension. At $r = r_o + H$, since the deformable solid is perfectly bonded to the rigid solid, disturbances must vanish

$$\tilde{u}_r = 0; \quad \tilde{u}_\theta = 0; \quad \tilde{u}_z = 0. \quad (28)$$

The above system of differential equations and boundary conditions are applicable to an arbitrary unidirectional flow in a cylindrical geometry subjected to non-axisymmetric disturbances and driven by the movement of a surface. To solve the above system of the differential equations and boundary conditions for the eigenvalue c, we use the pseudo-spectral method as discussed below.

A. Numerical methodology

In the pseudo-spectral method[26,27], we expand the dynamical quantities in terms of the Chebyshev polynomials as $\tilde{f}(y) = \sum_{m=0}^{m=N} a_m T_m(y)$ where $\tilde{f}(y), m, N, T_m(y)$ and a_m are respectively the fluid or solid eigenfunction, number of the Chebyshev polynomial, highest degree of the polynomial in the series expansion or the number of the collocation points, m^{th} Chebyshev polynomial and coefficient of m^{th} Chebyshev polynomial. Thus, we need to evaluate the series expansion at N collocation points to evaluate the series coefficients a_m and/or to obtain the eigenvalue c. The discretised matrices then form the eigenvalue problem of the following form

$$c^2\mathbf{C}\mathbf{e} + c\mathbf{B}\mathbf{e} + \mathbf{A}\mathbf{e} = 0. \tag{29}$$

where $\mathbf{A}, \mathbf{B}$ and $\mathbf{C}$ are the discretised matrices and $\mathbf{e}$ is the eigenvector. Next, we use the *polyeig* MATLAB routine to solve the above eigenvalue problem. To filter out the spurious modes in the numerically computed spectrum, the spectrum is obtained for N and $N + 2$ collocation points, and the eigenvalues are compared with a specified tolerance (e.g. 10^{-4}). The genuine eigenvalues are confirmed by changing the number of collocation points by 25 and observing the variation of the predicted eigenvalues. If the eigenvalue does not change up to sixth significant figure, we then use the same number of collocation points to predict the critical parameters. In the present work, $N = 75$ is found to be sufficient to predict the most unstable converged eigenvalue within the parameter range studied here.

III. RESULTS AND DISCUSSION

A. Validation

To validate our numerical method, we compare the eigenvalues reported in the literature with those predicted by the present numerical procedure. Since previous studies[7,9,11] considered the sliding Couette flow through an annulus having rigid wall, here we consider $\Gamma = 10^{-6}$ and $H = 0.01$ which effectively replaces the deformable wall with a rigid wall. Table I shows very good agreement between the present work and previous studies for the least stable eigenvalue thereby validating numerical methodology utilized in the present work. Table I also leads to conclusion that with increase in Re, the number of collocation points required for the convergence of the eigenvalues also increases. For $Re < 1000$, $N = 75$ is sufficient to resolve the spectrum and the eigenvalues are accurate up to five significant figures. In the present study, we are concerned about the stability of the flow for $Re < 1$, thus $N = 75$ is sufficient to resolve the spectrum. Figure 2 illustrates the change in the spectrum with respect to increase in the number of collocation points.

B. Creeping-flow limit

To begin with, it is useful to estimate the Reynolds number regimes encountered in the medical procedures alluded to in the Introduction. These applications involve fluid flows at relatively low Reynolds number ($Re = \rho^* V^* R^*/\mu^*$) where $\rho^*, R = (r_o^* - r_i^*)/2, V^*$ and μ^* are the density, half annular thickness, velocity and viscosity, respectively which can be estimated as follows. The typical diameter of blood vessels diameter is estimated to be $\sim 25\,mm, \sim 5\,mm$ and $\sim 5\,mm$ respectively for the human aorta, arteries and veins[28]. The guide wire has diameter of $\sim 1\,mm$. The thickness of the blood vessel walls is $\sim 2\,mm, \sim 1\,mm$ and $\sim 0.5\,mm$ respectively for

	(n,k)	(η, Re)	N	kc
Liu and Liu (2012)	$(3,3)$	$(1/3, 1000)$	50	$0.19232143 - 0.12378071i$
Preziosi and Rosso (1990)	$(3,3)$	$(1/3, 1000)$	30	$0.1923 - 0.1238i$
Present work	$(3,3)$	$(1/3, 1000)$	50	$0.19232206 - 0.12378236i$
Present work	$(3,3)$	$(1/3, 1000)$	75	$0.19231968 - 0.12378240i$
Liu and Liu (2012)	$(0, 0.6546)$	$(0.1, 3.6 \times 10^6)$	150	$0.62980689 - 0.00000201i$
Deguchi and Nagata (2011)	$(0, 0.6546)$	$(0.1, 3.6 \times 10^6)$	140	$0.62980833 - 0.00000202i$
Present work	$(0, 0.6546)$	$(0.1, 3.6 \times 10^6)$	125	$0.62980682 - 0.00000198i$
Present work	$(0, 0.6546)$	$(0.1, 3.6 \times 10^6)$	150	$0.62980689 - 0.00000202i$

TABLE I. Least stable eigenvalues, kc (rounded off to eighth significant figure) reported by the previous studies for rigid outer cylinder agree well with the results from the numerical formulation of the present work obtained for $\Gamma = 10^{-6}, T = 0$ and $H = 0.01$.

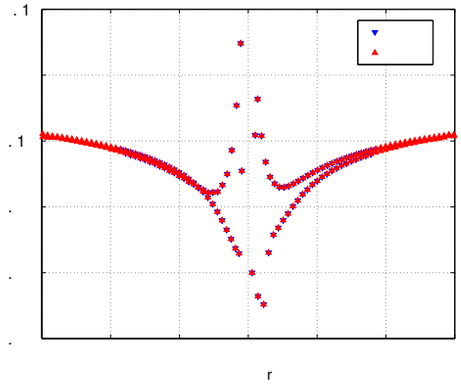

FIG. 2. Variation of the eigenspectrum with number of collocation points at $Re = 10, \beta = 0.5, \Gamma = 4, k = 0.5, H = 7, T = 0$ and $n = 1$. The least stable eigenvalues converge well with change in number of collocation points showing that for $Re < 10$, $N = 50$ is sufficient to analyze the stability of the flow.

the human aorta, arteries and veins[28]. Thus, half annulus thickness R^* is $\sim 6\,mm$ for the aorta and $\sim 1\,mm$ for arteries and veins. For blood flow through blood vessels, the density of blood, $\rho^* \sim 10^3 kg/m^3$ and the limiting viscosity of the blood is, $\mu^* \sim 0.01 Pa\,s$[29]. The velocity of the guide wire in the case of angioplasty is of $\sim 0.01\,m/s$[5,6]. Using these estimates, we determine the Reynolds number to be $O(1)$ in these applications, and thus restrict our discussion below to this regime.

Kumaran *et al.*[13] first predicted the existence of the finite-wave instability in the plane Couette flow past a linear viscoelastic solid which was later experimentally observed by Kumaran and Muralikrishnan[30]. The predicted finite-wave instability is characterized by critical dimensionless speed of the moving plate < 1 and critical wavenumber < 1. Since the plane Couette flow considered by Refs. 13 is a limiting case of the sliding Couette flow in the limit of narrow annular gap, we expect existence of the finite-wave instability for the present flow geometry in the narrow-gap limit.

Figure 3 shows the existence of the finite-wave instability in c_i vs k plot for $\Gamma > 1$. It must be noted that in our study the length scale is $R^* = (r_o^* - r_i^*)/2$, but for Kumaran *et al.*[13], the equivalent length scale is $(r_o^* - r_i^*)$. Thus, we arrive at the relation $\Gamma = 2\Gamma_K$ where Γ_K is the

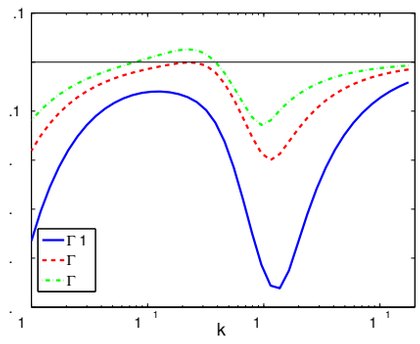

(a) c_i vs k at $\beta = 0.8$

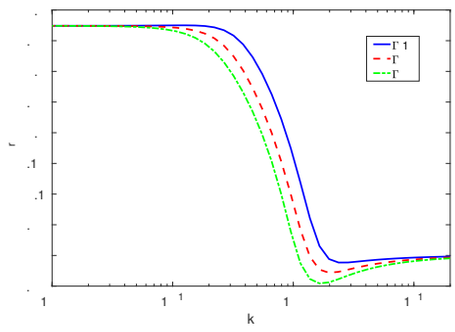

(b) c_r vs k at $\beta = 0.8$

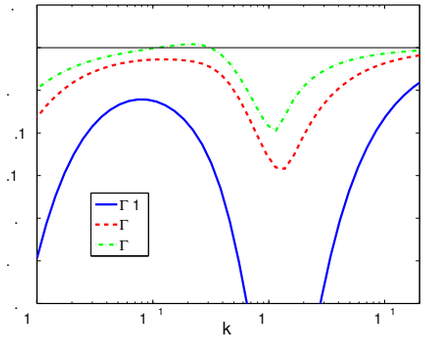

(c) c_i vs k at $\beta = 0.3$

FIG. 3. Variation of c_r and c_i of the most unstable (or least stable) mode at $Re = 0, H = 7, T = 0$ and $n = 0$. Panels (a) and (c) illustrate variation of the growth rate of the disturbances with the wavenumber while panel (b) shows the wavespeed of the disturbances with growth rate. This panel demonstrates the switching of the most unstable mode from the finite-wave mode to the short-wave mode at $k \sim O(1)$. Figure shows the existence of the finite-wave instability in the creeping-flow limit since $c_i > 0$ for $0.09 < k < 0.5$.

dimensionless shear rate for the plane Couette flow defined in the study of Kumaran *et al.*[13]. This indicates that, in the present case finite-wave instability must exist for the critical dimensionless speed of the moving cylinder (Γ_c) < 2. From figure 3(a), $\Gamma_c < 2$ in agreement with the prediction of Kumaran *et al.*[13]. However, from figure 3(c), with increase in annular gap i.e. decrease in β, Γ_c exceeds the characteristic $\Gamma_c < 2$ limit for the existence of the finite-wave instability. The existence of $\Gamma_c > 2$ for the finite-wave instability is a consequence of the increasing annular gap from very small annular gap limit expected for plane Couette flow. Thus, the finite-wave instability predicted for the plane Couette flow is somewhat stabilized due to increase in the annular gap width. The higher annular gap is important since as guide wire of the catheter in angioplasty moves through different size blood vessels, the annular gap varies which effectively makes the conclusions based on the plane Couette flow insufficient. This implies that to draw meaningful conclusions about the stability of the fluid flows encountered in the medical procedures, stability analysis of the sliding Couette flow is important.

To understand the effect of the variation in β and n on the finite-wave instability, we plot neutral stability curves in figure 4. These curves show that for the finite-wave instability $k_c < 1$ but Γ_c can exceed 2 depending on β and n. Thus, the instability predicted here can be understood to be the continuation of the instability for the plane Couette geometry to the sliding Couette geometry.

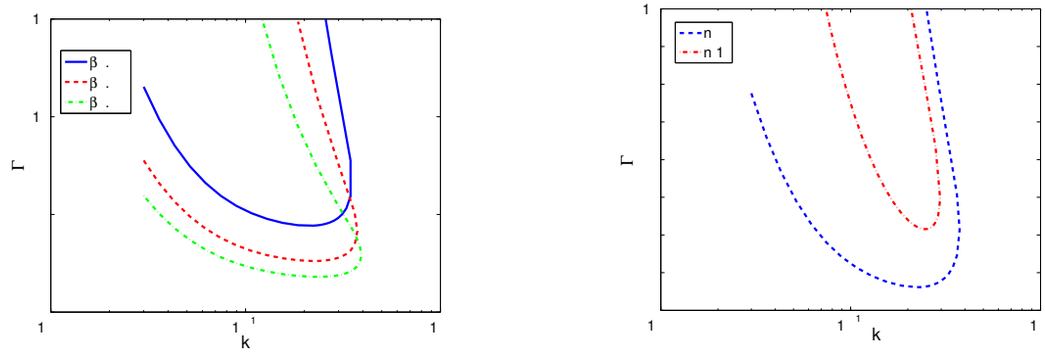

(a) $n = 0$ (b) $\beta = 0.6$

FIG. 4. Neutral stability curves (i.e. envelopes with $c_i = 0$) in Γ–k plane for the finite-wave mode at $Re = 0, T = 0$ and $H = 7$. Panels (a) and (b) respectively show the effect of variation in β and n on the finite-wave instability. The region on the concave side of the curves is unstable.

Furthermore, from figure 4(b), the finite-wave mode corresponding to axisymmetric disturbances is the most unstable one. In fact, for $H = 7, \beta = 0.6$ and $n > 1$, the finite-wave mode is linearly stable. We also point out an interesting contrast of the present prediction of instability in the creeping-flow limit for sliding Couette flow with the prediction of stability of finite-wave modes in pressure-driven flow in a deformable tube[16]. While both the geometries involve a cylindrical tube lined with deformable wall, the presence of pressure gradient in the latter configuration appears crucial in making the finite-wave modes flow stable in the creeping-flow limit.

Gkanis and Kumar[14], for the first time, performed a linear stability of the plane Couette flow past a neo-Hookean solid. The necessity to employ the neo-Hookean model arises because of the presence of the finite base state deformations when the flow is unstable. The study of Gkanis and Kumar[14] predicted existence of a short-wave instability characterized by $k_c > 1$ and $\Gamma_c > 2$ in terms of the present non-dimensionalization scheme. The short-wave instability arises because of the discontinuity in the first normal stress difference across the fluid-deformable-solid interface which is proportional to $\left(\frac{d\bar{u}_z}{d\bar{r}}\right)^2$. For a neo-Hookean solid, the first normal stress difference exists in any shearing deformation, it is expected that short-wave instability will be present in the present flow configuration as well. Other studies involving pressure-driven flows past deformable surface[17,31–33] have confirmed the presence of the short-wave instability.

Figure 5 illustrates the presence of the short-wave instability in sliding Couette flow for the axisymmetric disturbances. The neutral stability curves for the short-wave instability for two representative values of β are shown in figure 6(a). As expected, for the short-wave instability, $k_c > 1, \Gamma_c > 2$. Although, figure 5 shows $\Gamma_c > 5$ but for $T = 0$ and $\beta = 0.95$, the critical shear rate is $\Gamma_c \sim 2$ in agreement with the results for plane Couette flow[14]. In the previous studies involving cylindrical flow geometries such as Hagen-Poiseuille flow through a neo-Hookean tube[17,25,33], the short-wave instability has never been studied for the non-axisymmetric disturbances. For the first time, here we analyze the stability of the effect of the non-axisymmetric disturbances on the short-wave instability. Interestingly, for the short-wave instability from figure 6(b), the non-axisymmetric mode for $n = 4$ is the critical mode of the instability. This shows the importance of studying the stability of the sliding Couette flow subjected to the non-axisymmetric disturbances.

From figure 4(b) for $\beta = 0.6$, we concluded that axisymmetric perturbations are the critical mode of the instability for the finite-wave instability. However, this trend may change for higher

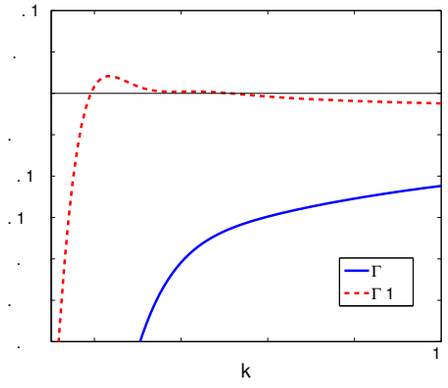

FIG. 5. Variation of c_i of the most unstable (or least stable) mode at $Re = 0, H = 0.5, \beta = 0.8, T = 1$ and $n = 0$. Figure shows existence of the short-wave instability in the creeping-flow limit.

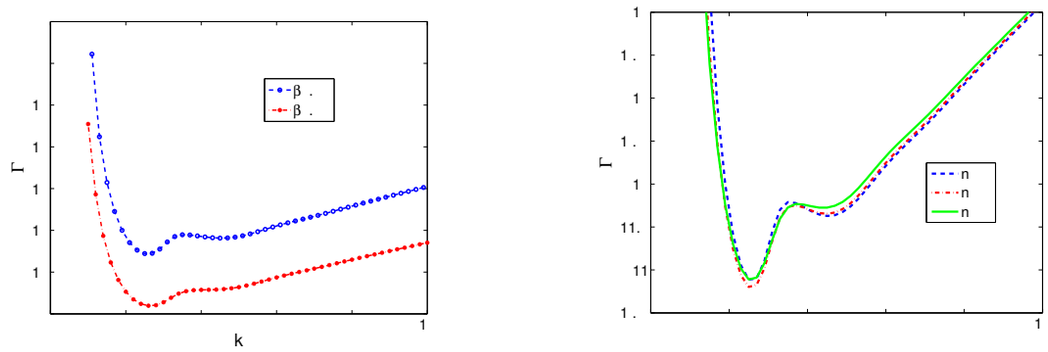

(a) $n = 0$ (b) $\beta = 0.6$

FIG. 6. Neutral stability curves in the Γ–k plane for the finite-wave mode at $Re = 0, T = 1$ and $H = 0.5$. Panels (a) and (b) respectively show the effect on short-wave instability due to variation in β and n.

gap between the cylinders due the variation of the thickness of the fluid layer. Figure 7(a) shows the variation of Γ_c with β for increasing n. In agreement with figure 4(b), figure 7(a) shows that axisymmetric mode is the critical mode for the finite-wave instability for arbitrary value β. Furthermore, as $\beta \to 1$ the axisymmetric and non-axisymmetric modes converge to Γ_c value for the plane Couette flow. This indicates that when fluid layer thickness is very small, axisymmetric and non-axisymmetric modes are destabilized simultaneously. From figure 7(a) since axisymmetric disturbances is the critical mode, henceforth we will study only the axisymmetric modes for the finite-wave instability.

Following earlier studies[13,14,30,31,34] on the stability of the fluid flow past deformable surfaces, here we study the variation of the critical parameters with H for the finite-wave instability in figure 8. The critical parameters show the scaling $\sim 1/H$ for $H > 5$ which is also one of the characteristic feature of the finite-wave instability. Additionally, we find that increasing β has destabilizing effect on the finite-wave instability in agreement with figure 7(a).

Similar to the finite-wave instability, figure 9 shows the variation of Γ_c with β for $H = 0.5$. Unlike the finite-wave instability, for the short-wave instability critical mode is the non-axisymmetric mode $n = 4$, in agreement with the results of figure 6(b). Interestingly, decreasing β has a stabiliz-

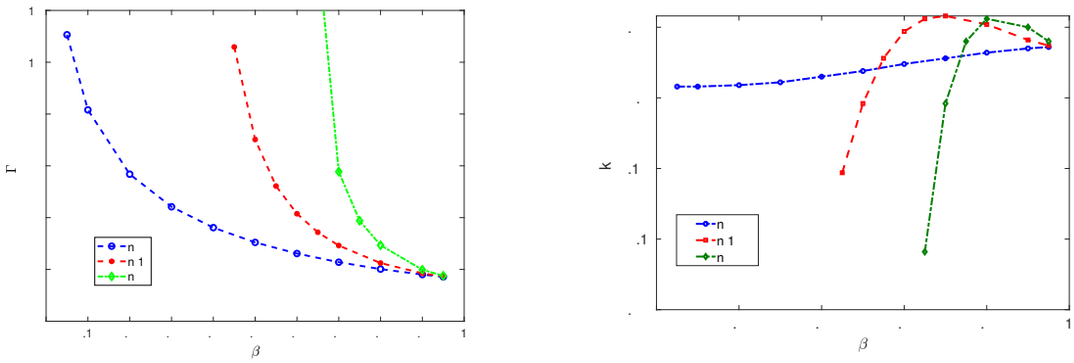

(a) Γ_c vs β (b) k_c vs β

FIG. 7. Panels (a) and (b) respectively show the variation of the critical parameters with β for the finite-wave instability at $Re = 0, T = 0$ and $H = 7$. The axisymmetric mode is the critical mode for the finite-wave instability.

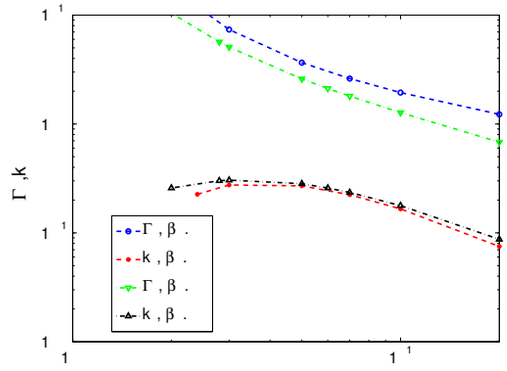

FIG. 8. Variation of the critical parameters with H for $Re = 0, T = 0$ and $n = 0$. For high H, $k_c, \Gamma_c \sim 1/H$.

ing effect on both axisymmetric and non-axisymmetric disturbances, but the former is stabilized faster than latter. This relatively faster stabilization of the axisymmetric modes makes the non-axisymmetric mode with $n = 4$ the critical mode for the short-wave instability. As $\beta \to 1$, Γ_c for the axisymmetric and non-axisymmetric asymptote to Γ_c for the plane Couette flow. Thus, similar to the finite-wave disturbances, the axisymmetric and non-axisymmetric short-wave disturbances are triggered simultaneously when the annular gap is sufficiently small. Furthermore, the difference between the critical parameters widens as β decreases. To conclude, axisymmetric mode is the critical mode for the finite-wave instability while non-axisymmetric mode ($n = 4$) is the critical mode for the short-wave instability.

The short-wave mode of perturbations for $n = 4$ are shown in figure 10 at marginal stability parameters. The perturbations are normalised by the maximum absolute value of the corresponding eigenfunctions. In figure 10(a), at $r = 0$ which translates to $r = r_i$ in physical space, v_z' vanishes, as required by the boundary conditions at the moving cylinder. This is likewise true for u_z', where the disturbances must vanish at $r = r_o + H$, which corresponds to $r = 0$ in figure 10(b). The

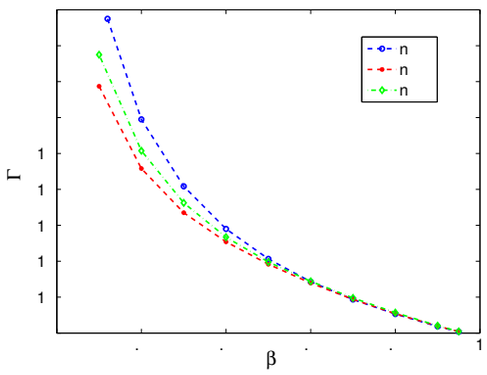

FIG. 9. Variation of the critical parameters with β for $Re = 0, T = 1$ and $H = 0.5$. The non-axisymmetric mode with $n = 4$ is the critical mode for the short-wave instability. The results are obtained for a fixed $k = 20$ since for the short-wave instability, the variation in critical parameters beyond $k = 20$ is found to be negligible.

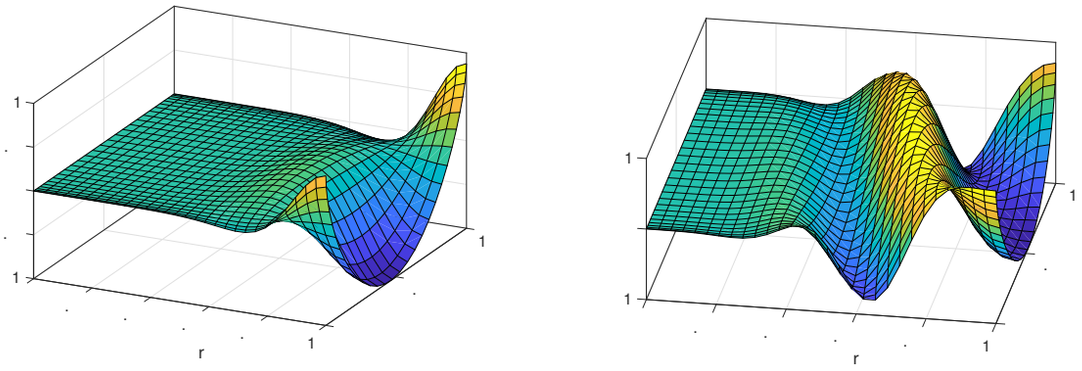

(a) v_z' (b) u_z'

FIG. 10. The normalized short-wave perturbations for the fluid and deformable solid at $Re = 0, T = 1, n = 4, \Gamma = 9.9, k = 5$ and $H = 0.5$ for the marginally stable short-wave mode $c = -0.038215$. Here, $v_z' = Re\left[\tilde{v}_z e^{ikz}\right]$ (panel a) and $u_z' = Re\left[\tilde{u}_z e^{ikz}\right]$ (panel b). For convenience, the axes for the fluids and deformable solid have been normalized to the interval $[0, 1]$. The length of the domain in the z-direction is equal to a wavelength $(2\pi/k)$ of the perturbations. The plots illustrates the twisting motion induced by the non-axisymmetric mode for $n = 4$.

fluid-deformable solid interface is present at $r = 1$ in both panels of figure 10.

The short-wave instability arises due to the existence of the first normal-stress difference exhibited by the neo-Hookean solid. The non-axisymmetric mode corresponding to $n = 4$ will lead to a twisting-type of motion at the fluid-deformable solid interface as illustrated in figure 10. We expect that a constructive interaction between the twisting motion introduced by the non-axisymmetric mode and the first normal stress difference gives rise to a lesser Γ_c for $n = 4$ mode. However, for the non-axisymmetric modes corresponding to higher n might cause a destructive interaction between the twisting motion and the first normal stress difference thereby increasing Γ_c. It must be noted that the first normal stress difference is indeed important since the axisymmetric mode is the

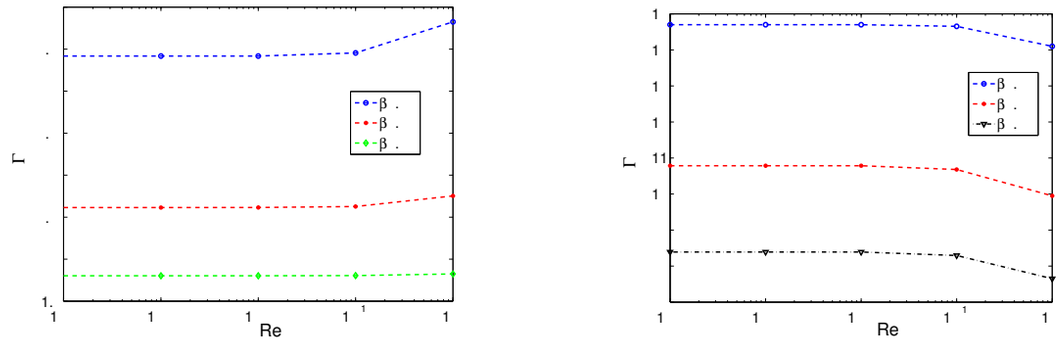

(a) Finite-wave instability for $n = 0, T = 0$ and $H = 7$

(b) Short-wave instability for $n = 4, T = 1$ and $H = 0.5$

FIG. 11. Panels (a) and (b) respectively show the variation of the critical parameters with Re for the finite-wave ($n = 0, T = 0$ and $H = 7$) and short-wave ($n = 4, T = 1$ and $H = 0.5$) instabilities. Inertia has stabilizing effect on the finite-wave instability while destabilizing effect on the short-wave instability.

most unstable mode for the finite-wave instability for which the the first normal stress difference does not play a major role.

C. Effect of inertia ($Re \neq 0$)

The preceding discussion corresponds to the stability of the flow in the creeping-flow limit. In this section, we study the effect of the increase in inertia on the finite-wave and short-wave instabilities. From figure 11, increasing inertia has small stabilizing effect on the finite-wave instability while destabilizing effect on the short-wave instability. In the case of finite-wave instability, the stabilizing effect increases with decreasing β. However, for the short-wave instability the destabilizing effect of the increasing inertia is independent of β. It must be noted that the wall and inviscid modes of the instability reported in the literature[17,30,32–34] related to the flow past deformable surfaces are stable for $Re < 1$. Thus, for small Re (< 1), the stability of the flow is determined by the finite-wave and short-wave instabilities discussed above.

D. Role of an unrestrained boundary at $r = r_o + H$

As mentioned in the Introduction, in medical procedures such as angioplasty and thread injection, the blood vessel plays the role of the outer deformable cylinder, and these are not rigidly bonded to an outer rigid cylinder. In such cases, to mimic the physiologically relevant conditions, we replace the boundary conditions (Eq. 28) with stress-free boundary conditions. A rigorous treatment of this configuration using the neo-Hookean model is mathematically and computationally cumbersome. Thus, in what follows, we use the linear elastic model for the deformable solid layer to illustrate the qualitative effects of an unrestrained boundary. The use of the linear elastic model for the present problem can be justified as follows.

For $H \geq 2$, the study of Gkanis and Kumar[14] on the plane Couette flow past a neo-Hookean solid shows that the result obtained from linear elastic and neo-Hookean models are in excellent agreement. However, for $H <$, for plane Couette flow past a deformable solid, Γ_c, is sufficiently

high such that deviations appear in results obtained by linear elasticity, compared with a neo-Hookean model. However, this is not an issue in the present analysis since the finite-wave instability predicted here for $H < 1$ exists at low values of $\Gamma\,(< 0.1)$, for which linear elasticity and more advanced models such as the neo-Hookean model are in good agreement[14,32,35]. Therefore, linear elasticity is deemed sufficient to describe the dynamics of the deformable solid layer, and hence to study the linear stability of the present system for the unrestrained boundary.

In practice, the unrestrained deformable annular cylinder is tethered at the two ends. For this case, a tangential stress at the fluid-deformable solid interface will then lead to deformation field that varies with the axial direction in the deformable wall. However, a rigorous consideration of such a configuration necessitates a global stability analysis. The case of steady flow with induced pressure in the deformable wall has been studied by Shankar and Kumaran[36]. Recently, Mandloi and Shankar[22] studied a pressure driven plane Poiseuille flow through a deformable channel with one unrestrained boundary. Here, we assume that the deformation developed in the deformable walls is negligible, and hence the use of a linear elastic model is justified. Thus, the present analysis is an attempt to demonstrate the qualitative role of unrestrained vessel walls in introducing instabilities.

The governing equations for the linear elastic solid can be readily obtained from equations (18-20) by substituting $D\bar{u}_z = 0$. A similar substitution in the fluid-solid interface conditions (25-27) results in the corresponding interface conditions for a linear elastic solid. While, the boundary conditions (28) at $r = r_o + H$ due to the unrestrained condition become

$$\frac{1}{\Gamma} D\tilde{u}_z + \frac{ik}{\Gamma}\tilde{u}_r = 0, \tag{30}$$

$$\frac{1}{\Gamma}\left(D - \frac{1}{r_o + H}\right)\tilde{u}_\theta + \frac{in}{\Gamma(r_o + H)}\tilde{u}_r = 0, \tag{31}$$

$$-\tilde{p}_s + \frac{2}{\Gamma} D\tilde{u}_r = 0. \tag{32}$$

The pseudo-spectral code is then modified accordingly to compute the eigenvalues and carry out the subsequent analysis.

The unrestrained boundary reduces the critical parameter Γ_c to $O(10^{-4})$ or even lower, depending on the length and thickness of the deformable cylinder, as shown in Fig. 12. The wavelength of the unstable mode is determined by the length of the deformable cylinder (L) since the most unstable modes correspond to $k \to 0$. Thus, in the medical procedures where $H \sim O(0.1)$ and Γ_c is very low, the predicted instability is expected to be relevant.

IV. CONCLUDING REMARKS

In the present study, we showed using a linear stability analysis that sliding Couette flow of a Newtonian fluid in the gap between two concentric cylinders with a deformable wall is unstable even in the creeping-flow limit and at very low Reynolds number ($Re < 1$). This is in direct contrast with sliding Couette flow with rigid walls, which is linearly unstable only for $\beta < 0.1415$ and $Re_c \sim O(10^6)$. The sliding Couette flow exhibits finite-wave and short-wave instabilities even in the creeping-flow limit as a consequence of the deformable wall. Further, the axisymmetric mode is the critical mode for the finite-wave instability, since critical dimensionless velocity (Γ_c) required for it is lower than that for the non-axisymmetric modes. However, for the short-wave instability, the non-axisymmetric mode with $n = 4$ is the critical mode. Increase in the gap between the two cylinders (or, decrease in β) has a stabilizing effect on the both class of the

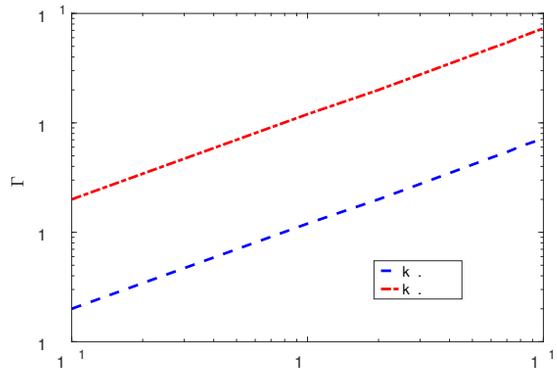

FIG. 12. Variation of Γ_c with β for $Re = 0, T = 0$ and $\beta = 0.6$. The finite-wave mode due to the unrestrained boundary at $r = r_o + H$ becomes unstable at much lower Γ_c than for a restrained boundary.

instabilities. Increase in inertia, however, has stabilizing and destabilizing effects respectively on finite-wave and short-wave instabilities.

To mimic the flows involved in medical procedures, we also considered an unrestrained deformable wall which predicts the finite-wave instability at much lower Γ_c compared to the restrained configuration. Overall, the stability characteristics of the sliding Couette flow with a deformable wall are drastically different from those for the corresponding configuration with a rigid wall. Our results therefore suggest that in practical applications involving sliding Couette flow, the deformability of the wall is expected to play a vital role in determining stability of the system. Important questions of relevance to future work include a spatio-temporal analysis to explore the possibility of absolute instability in this configuration, as well as a non-modal stability analysis to understand the possibility of transient growth in regimes where the flow is stable.

Data Availability: The data that support the findings of this study are available from the corresponding author upon reasonable request.

REFERENCES

[1]Z. Tadmor and R. B. Bird, "Rheological analysis of stabilizing forces in wire-coating dies," Polym. Eng. Sci. **14**, 124–136 (1974).
[2]M. S. Arney, R. Bai, E. Guevara, D. D. Joseph, and K. Liu, "Friction factor and holdup studies for lubricated pipelining. I. experiments and correlations." Intl J. Multiphase Flow **19**, 1061–1076 (1993).
[3]T. Vaskopulos, C. E. Polymeropoulos, and A. Zebib, "Heat transfer from optical fibre during the draw process," J. Mat. Proc. Manuf. Sci. **1**, 261–271 (1993).
[4]A. G. Walton, "The nonlinear instability of thread-annular flow at high Reynolds number," J. Fluid Mech. **477**, 227–257 (2003).
[5]A. G. Walton, "Stability of circular Poiseuille-Couette flow to axisymmetric disturbances," J. Fluid Mech. **500**, 169–210 (2004).
[6]A. G. Walton, "The linear and nonlinear stability of thread-annular flow," Phil. Trans. R. Soc. A **363**, 1223–1233 (2005).

[7]K. Deguchi and M. Nagata, "Bifurcations and instabilities in sliding Couette flow," J. Fluid Mech. **678**, 156–178 (2011).
[8]R. A. Byrne, G. W. Stone, J. Ormiston, and A. Kastrati, "Coronary balloon angioplasty, stents, and scaffolds," Lancet **390**, 781–92 (2017).
[9]L. Preziosi and F. Rosso, "Stability of a viscous liquid between sliding pipes," Phys. Fluids A: Fluid Dynamics **2**, 1158 (1990).
[10]P. Gittler, "Stability of axial Poiseuille-Couette flow between concentric cylinders," Acta Mechanica **101**, l–13 (1993).
[11]R. Liu and Q. S. Liu, "Non-modal stability in sliding Couette flow," J. Fluid Mech. **710**, 505–544 (2012).
[12]C. A. Daly and N. Peake, "Non-modal instability of annular Poiseuille-Couette flow," European Journal of Mechanics B/Fluids **53**, 148–159 (2015).
[13]V. Kumaran, G. H. Fredrickson, and P. Pincus, "Flow induced instability of the interface between a fluid and a gel at low Reynolds number," J. Phys. II France. **4**, 893–904 (1994).
[14]V. Gkanis and S. Kumar, "Instability of creeping couette flow past a neo-Hookean solid," Phys. Fluids **15**, 2864–2471 (2003).
[15]Gaurav and V. Shankar, "Stability of gravity-driven free-surface flow past a deformable solid layer at zero and finite Reynolds number," Phys. Fluids **19**, 024105 (2007).
[16]R. Patne and V. Shankar, "Absolute and convective instability in combined Couette-Poiseuille flow past a neo-Hookean solid," Phys. Fluids **29**, 124104 (2017).
[17]R. Patne and V. Shankar, "Stability of flow through deformable channels and tubes: implications of consistent formulation," J. Fluid Mech. **860**, 837–885 (2018).
[18]B. Dinesh and S. Pushpavanam, "Stability of stratified flows through neo-hookean soft-gel-coated walls," Physics of Fluids **30**, 104103 (2018).
[19]D. Giribabu and V. Shankar, "Stability of plane couette flow of a power-law fluid past a neo-hookean solid at arbitrary reynolds number," Physics of Fluids **29**, 074106 (2017).
[20]V. S. Tanmay, R. Patne, and V. Shankar, "Stability of plane couette flow of carreau fluids past a deformable solid at arbitrary reynolds numbers," Physics of Fluids **30**, 074103 (2018).
[21]P. Joshi and V. Shankar, "Flow-induced resonant shear-wave instability between a viscoelastic fluid and an elastic solid," Physics of Fluids **31**, 084107 (2019).
[22]S. Mandloi and V. Shankar, "Stability of flow in a deformable channel with an unrestrained boundary," Physics of Fluids **32**, 054107 (2020).
[23]V. Shankar, "Stability of fluid flow through deformable tubes and channels: An overview," Sadhana **40**, 925–943 (2015).
[24]V. Kumaran, "Experimental studies on the flow through soft tubes and channels," Sadhana **40**, 911–923 (2015).
[25]R. Patne, D. Giribabu, and V. Shankar, "Consistent formulations for stability of fluid flow through deformable channels and tubes," J. Fluid Mech. **827**, 31–66 (2017).
[26]J. P. Boyd, *Chebyshev and Fourier Spectral Methods*, 2nd ed. (Dover, New York, 2001).
[27]D. Gottlieb and S. A. Orszag, *Numerical Analysis of Spectral Methods* (SIAM, Philadelphia, 1977).
[28]B. Müller, S. Lang, M. Dominietto, M. Rudin, G. Schulz, H. Deyhle, M. Germann, F. Pfeiffer, C. David, and T. Weitkamp, "High-resolution tomographic imaging of microvessels," Proc. SPIE **7078**, 70780B (2008).
[29]C. Picart, J. M. Piau, H. Galliard, and P. Carpentier, "Human blood shear yield stress and its hematocrit dependence," J. Rheol. **42**, 1–12 (1998).
[30]V. Kumaran and R. Muralikrishnan, "Spontaneous growth of fluctuations in the viscous flow of

a fluid past a soft interface," Phys. Rev. Lett. **84**, 3310–3313 (2000).
[31]V. Gkanis and S. Kumar, "Stabilty of pressure-driven creeping flows in channels lined with a nonlinear elastic solid," J. Fluid Mech. **524**, 357–375 (2005).
[32]Gaurav and V. Shankar, "Stability of fluid flow through deformable neo-Hookean tubes," J. Fluid Mech. **627**, 291–322 (2009).
[33]Gaurav and V. Shankar, "Stability of pressure-driven flow in a deformable neo-Hookean channel," J. Fluid Mech. **659**, 318–350 (2010).
[34]P. Chokshi and V. Kumaran, "Weakly nonlinear analysis of viscous instability in flow past a neo-Hookean surface," Phys. Rev. E **77**, 056303 (2008).
[35]V. Shankar and S. Kumar, "Instability of viscoelastic plane Couette flow past a deformable wall," J. Non-Newtonian Fluid Mech. **116**, 371–393 (2004).
[36]V. Shankar and V. Kumaran, "Weakly nonlinear stability of viscous flow past a flexible surface," J. Fluid Mech. **434**, 337–354 (2001).

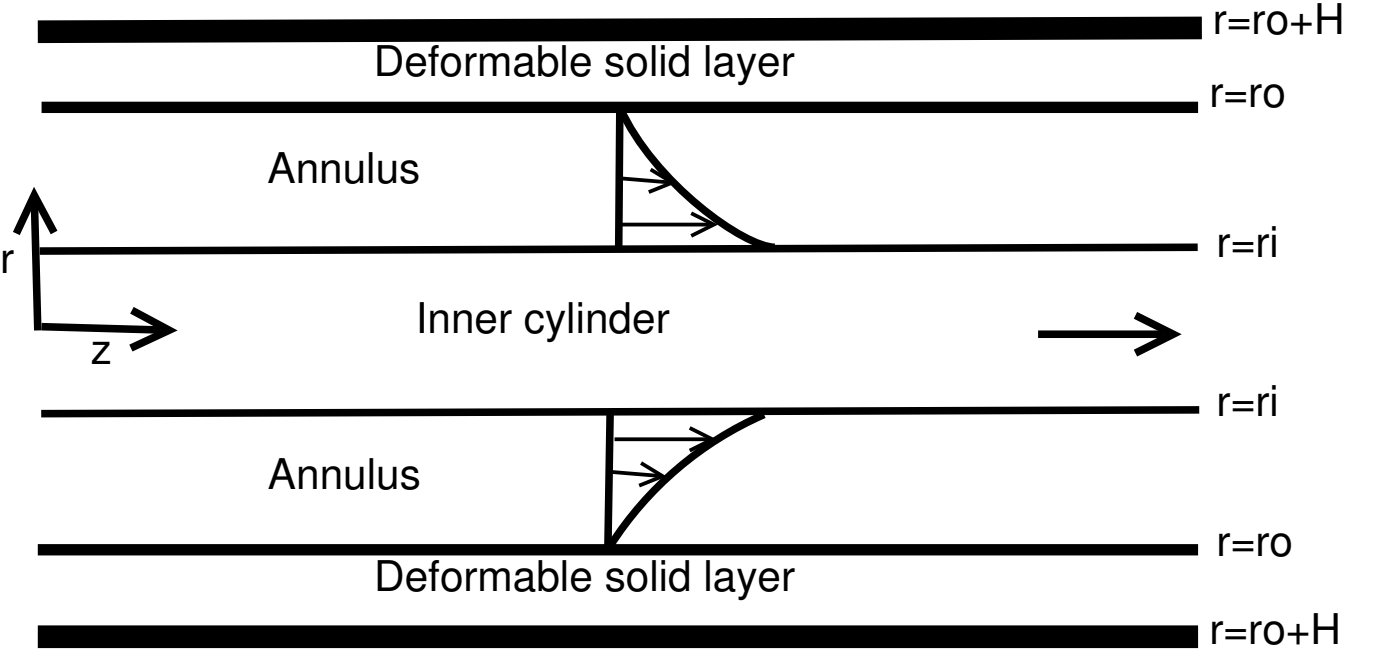
r=ro+H
Deformable solid layer
r=ro
Annulus
r=ri
r
z
Inner cylinder
r=ri
Annulus
r=ro
Deformable solid layer
r=ro+H

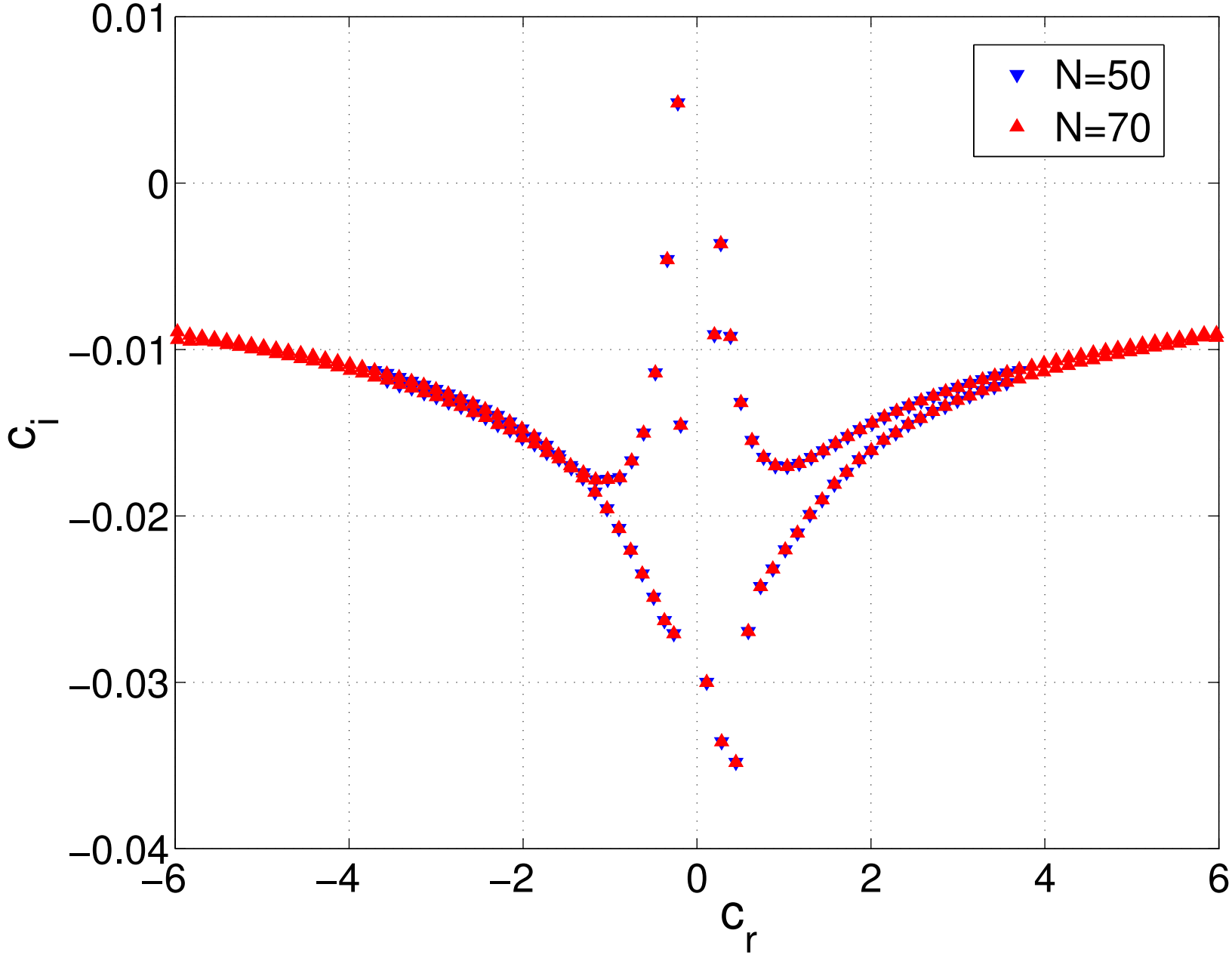
0.01
0
−0.01
−0.02
−0.03
−0.04
−6
−4
−2
0
2
4
6
c_i
c_r
N=50
N=70

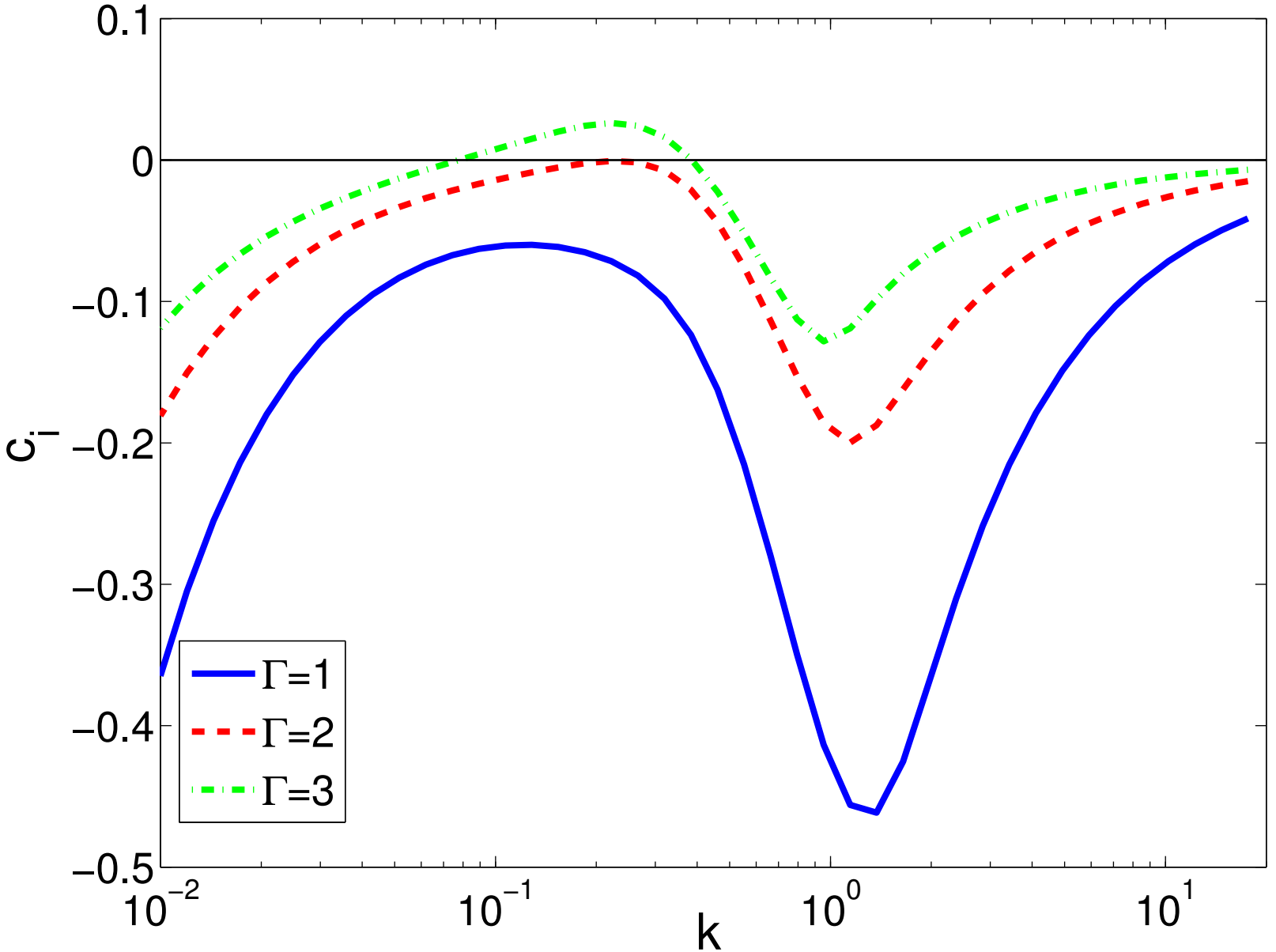
0.1
0
−0.1
−0.2
−0.3
−0.4
−0.5
c_i
10^{-2}
10^{-1}
10^{0}
10^{1}
k
Γ=1
Γ=2
Γ=3

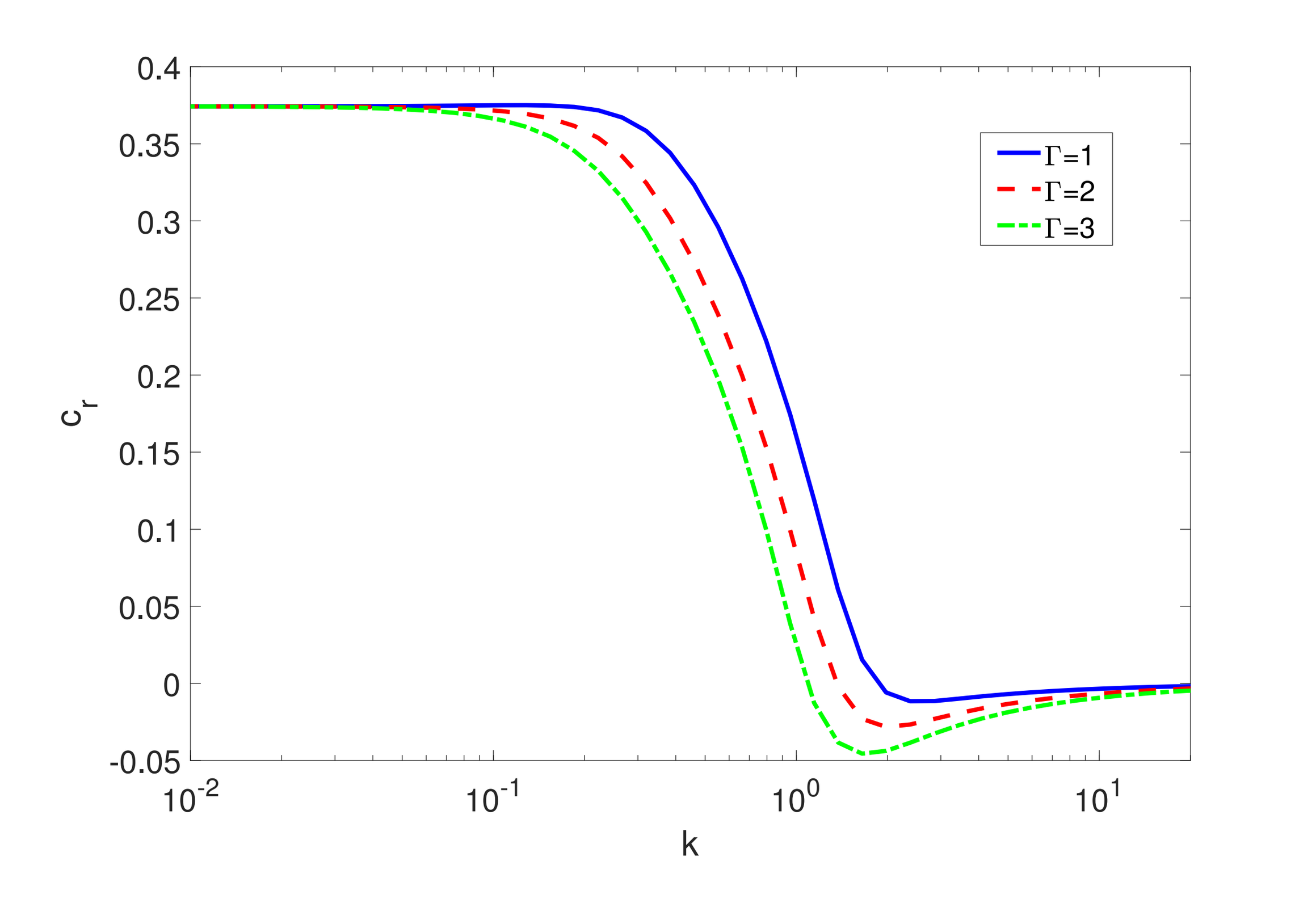
0.4
0.35
0.3
0.25
0.2
0.15
0.1
0.05
0
-0.05
c_r
10^{-2}
10^{-1}
10^{0}
10^{1}
k
Γ=1
Γ=2
Γ=3

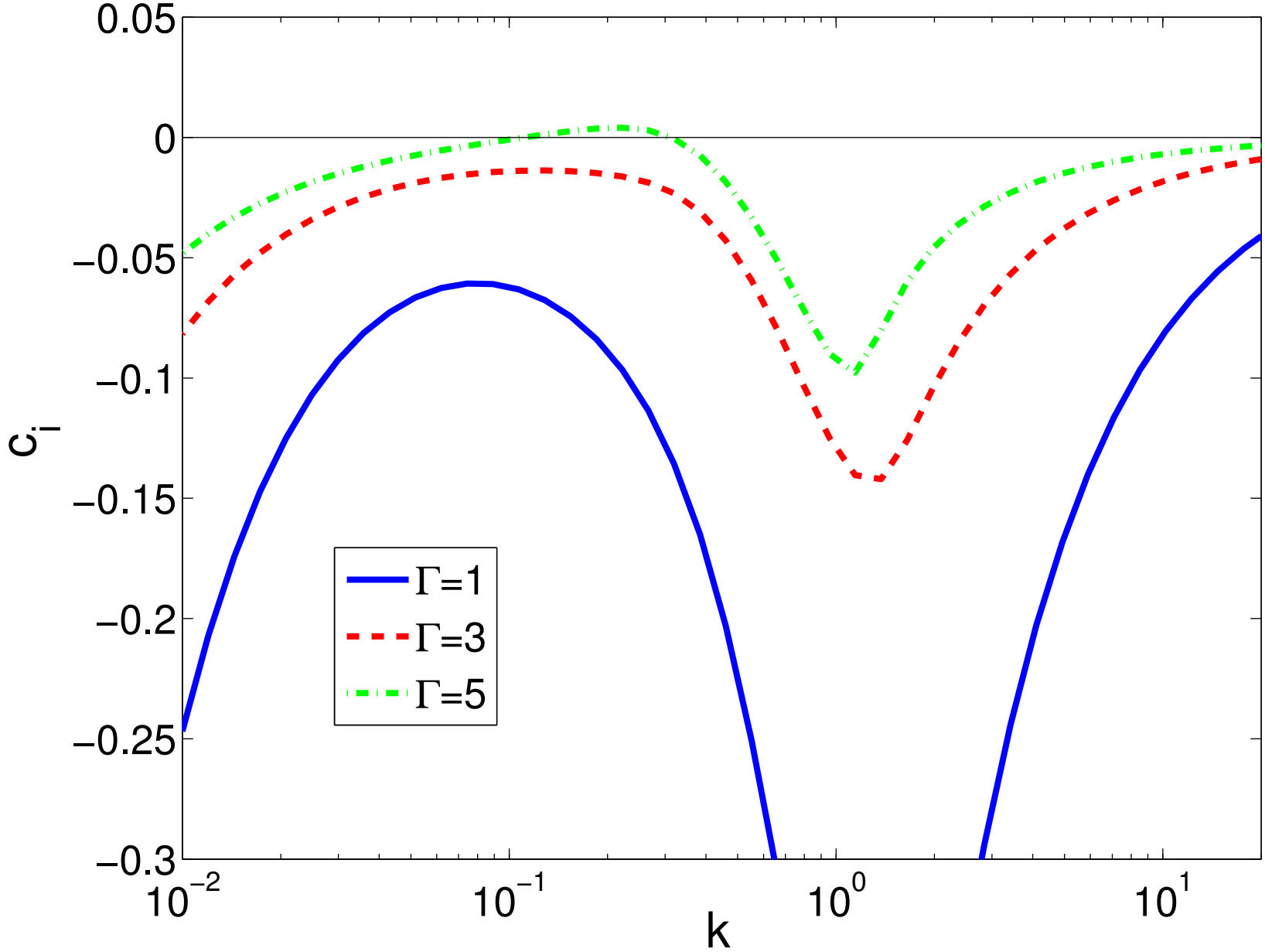
0.05
0
−0.05
−0.1
−0.15
−0.2
−0.25
−0.3
c_i
10^{-2}
10^{-1}
10^{0}
10^{1}
k
Γ=1
Γ=3
Γ=5

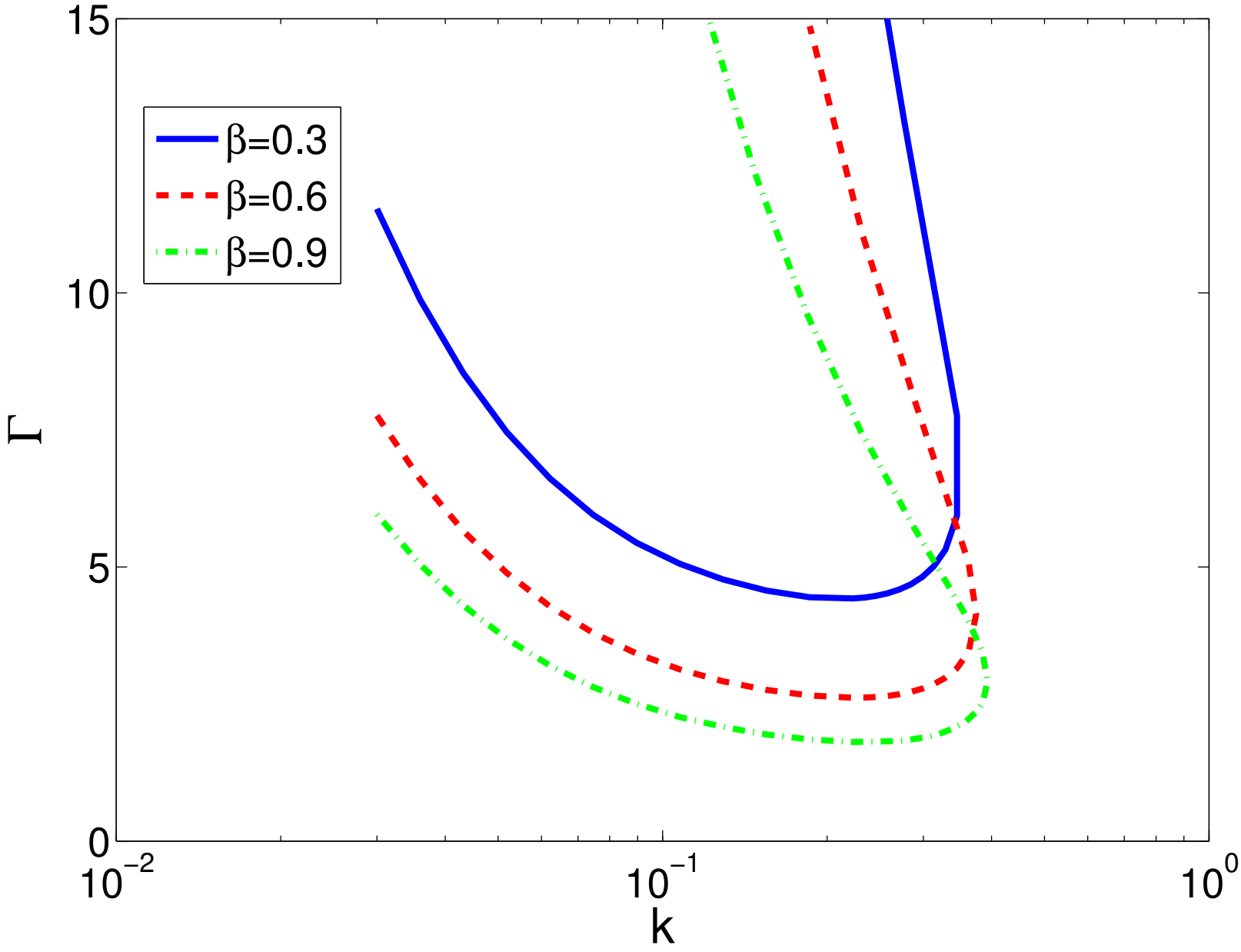
15
10
5
0
Γ
β=0.3
β=0.6
β=0.9
10^−2
10^−1
10^0
k

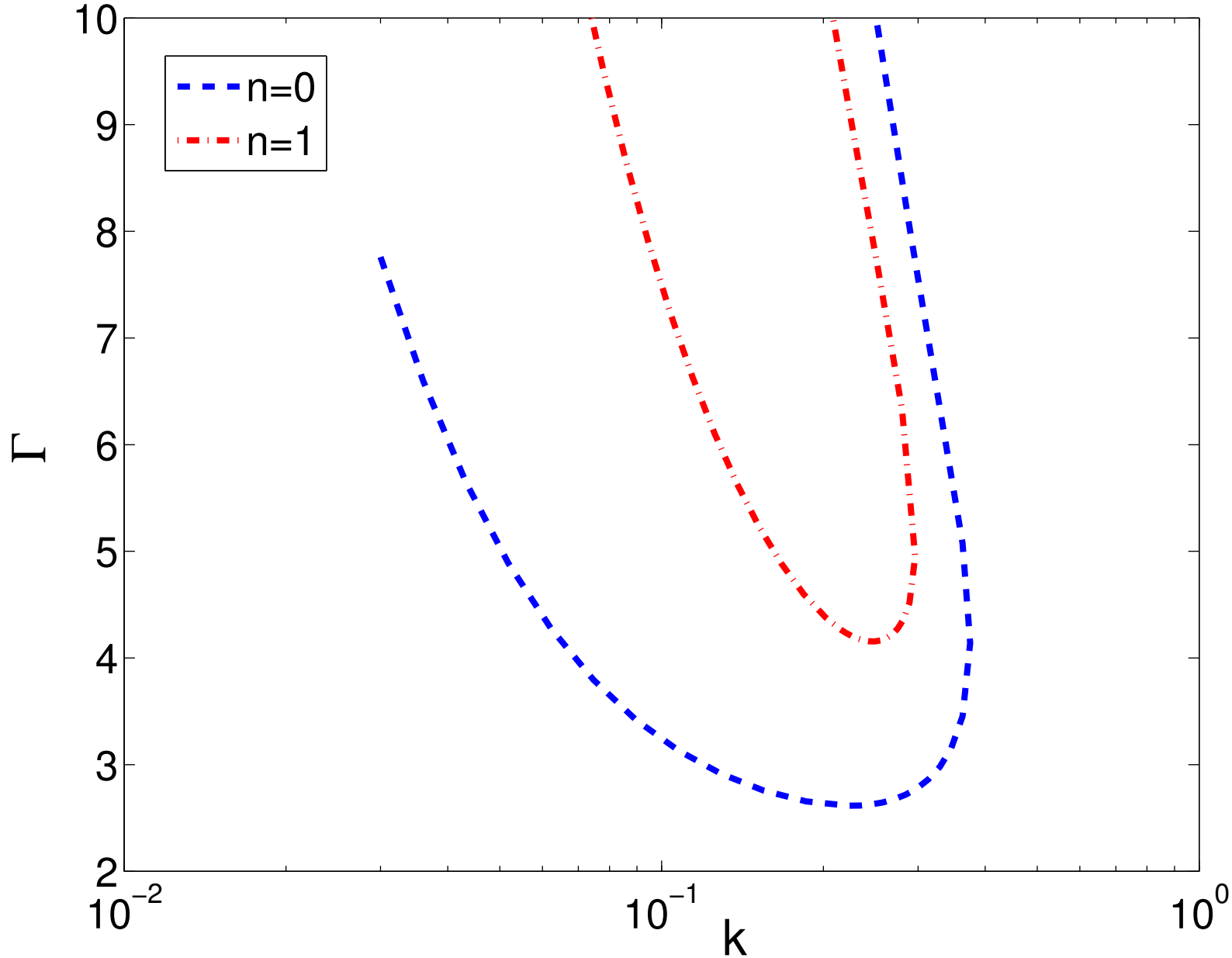
n=0
n=1
Γ
k
10
9
8
7
6
5
4
3
2
10^{-2}
10^{-1}
10^{0}

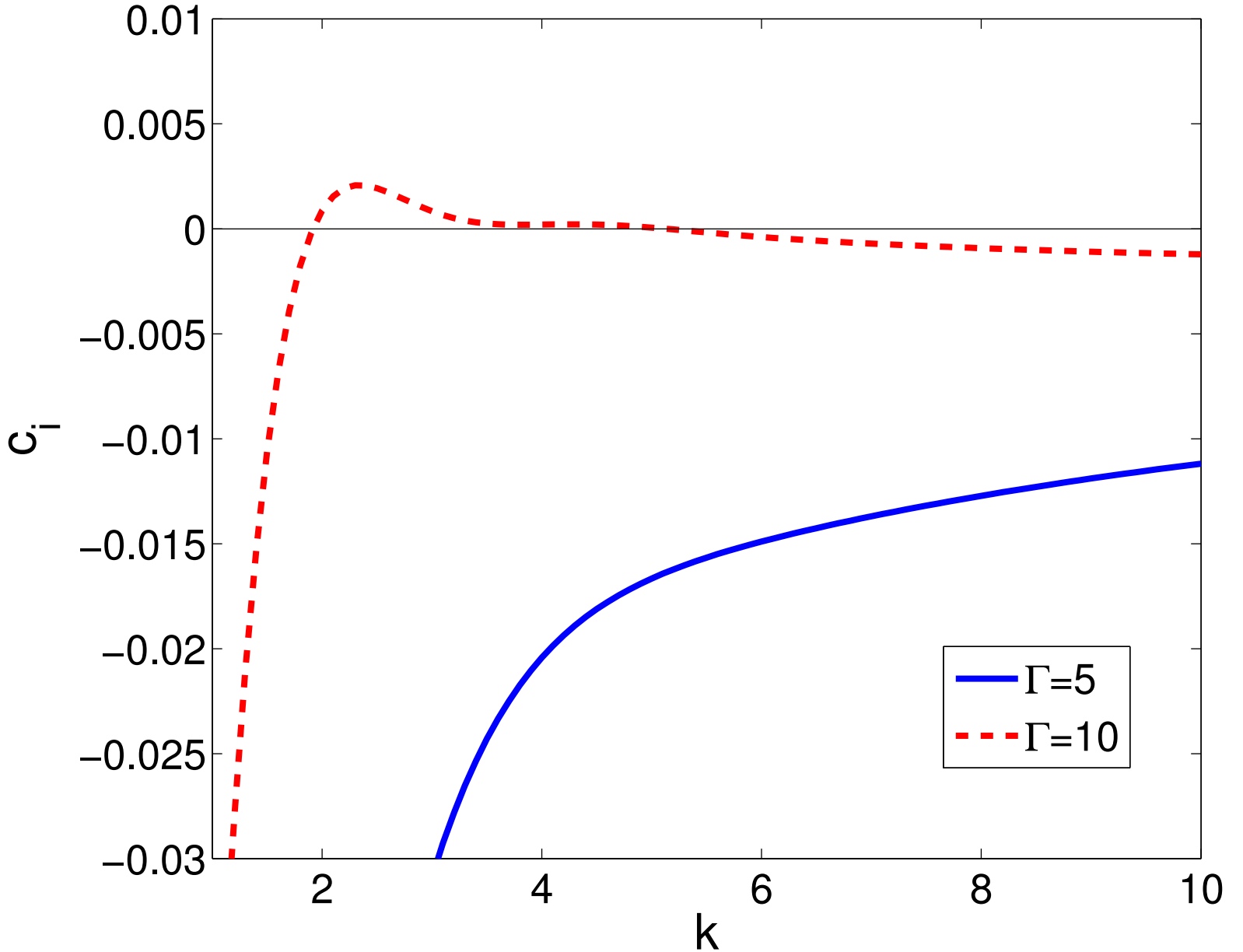
0.01
0.005
0
−0.005
−0.01
−0.015
−0.02
−0.025
−0.03
c_i
2
4
6
8
10
k
Γ=5
Γ=10

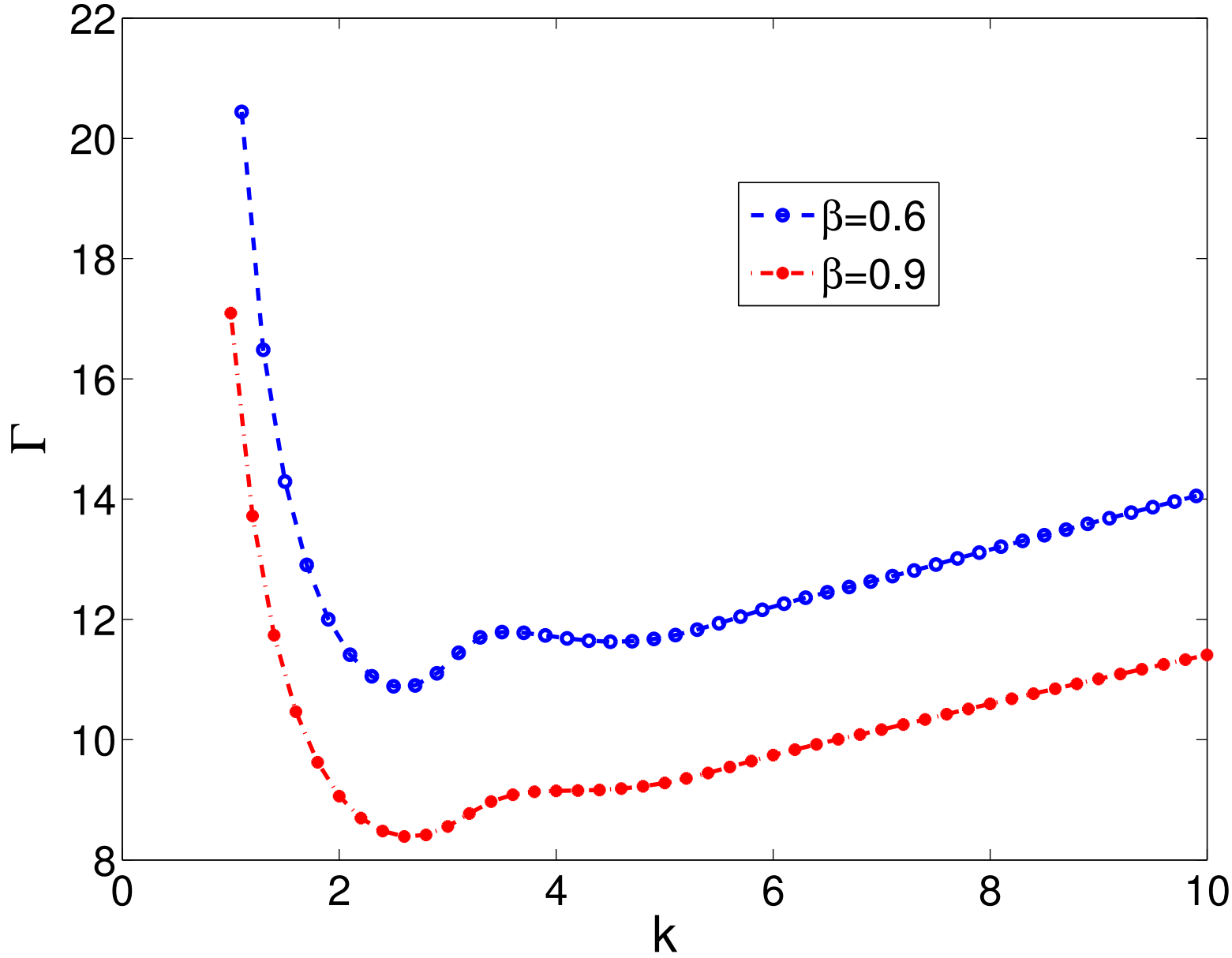
22
20
18
16
14
12
10
8
Γ
0
2
4
6
8
10
k
β=0.6
β=0.9

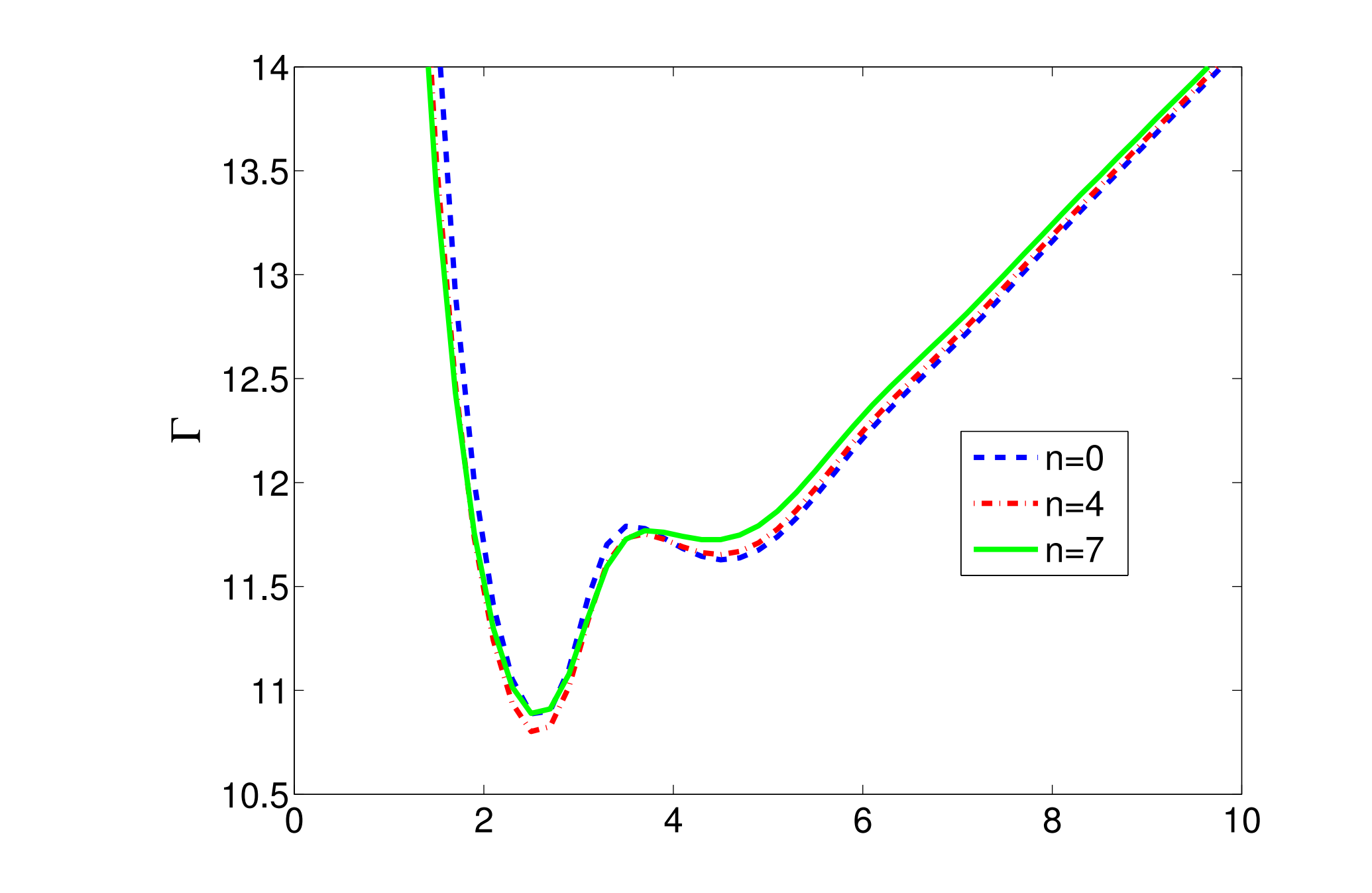
14
13.5
13
12.5
12
11.5
11
10.5
Γ
0
2
4
6
8
10
n=0
n=4
n=7

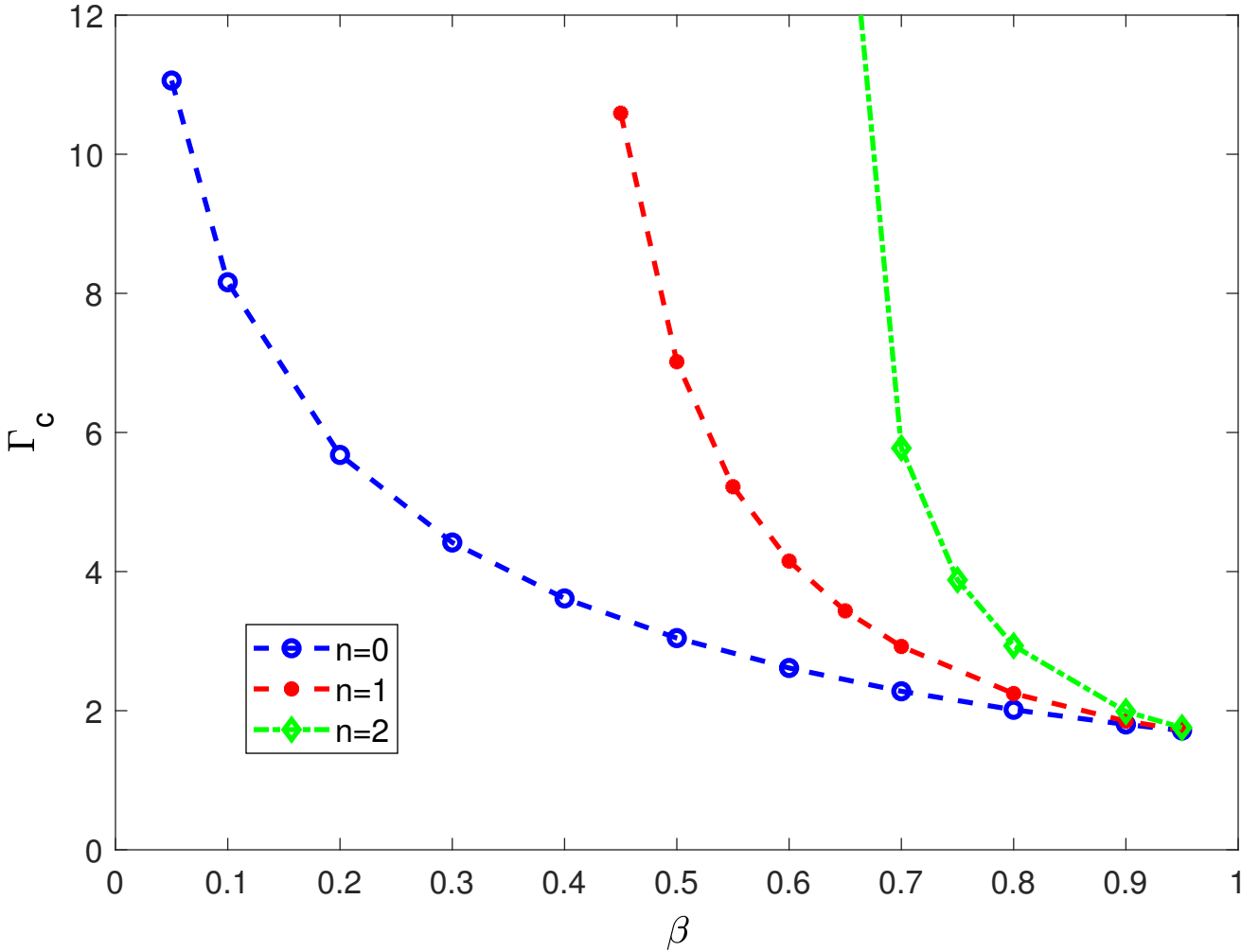
12
10
8
6
4
2
0
0
0.1
0.2
0.3
0.4
0.5
0.6
0.7
0.8
0.9
1
Γ_c
β
n=0
n=1
n=2

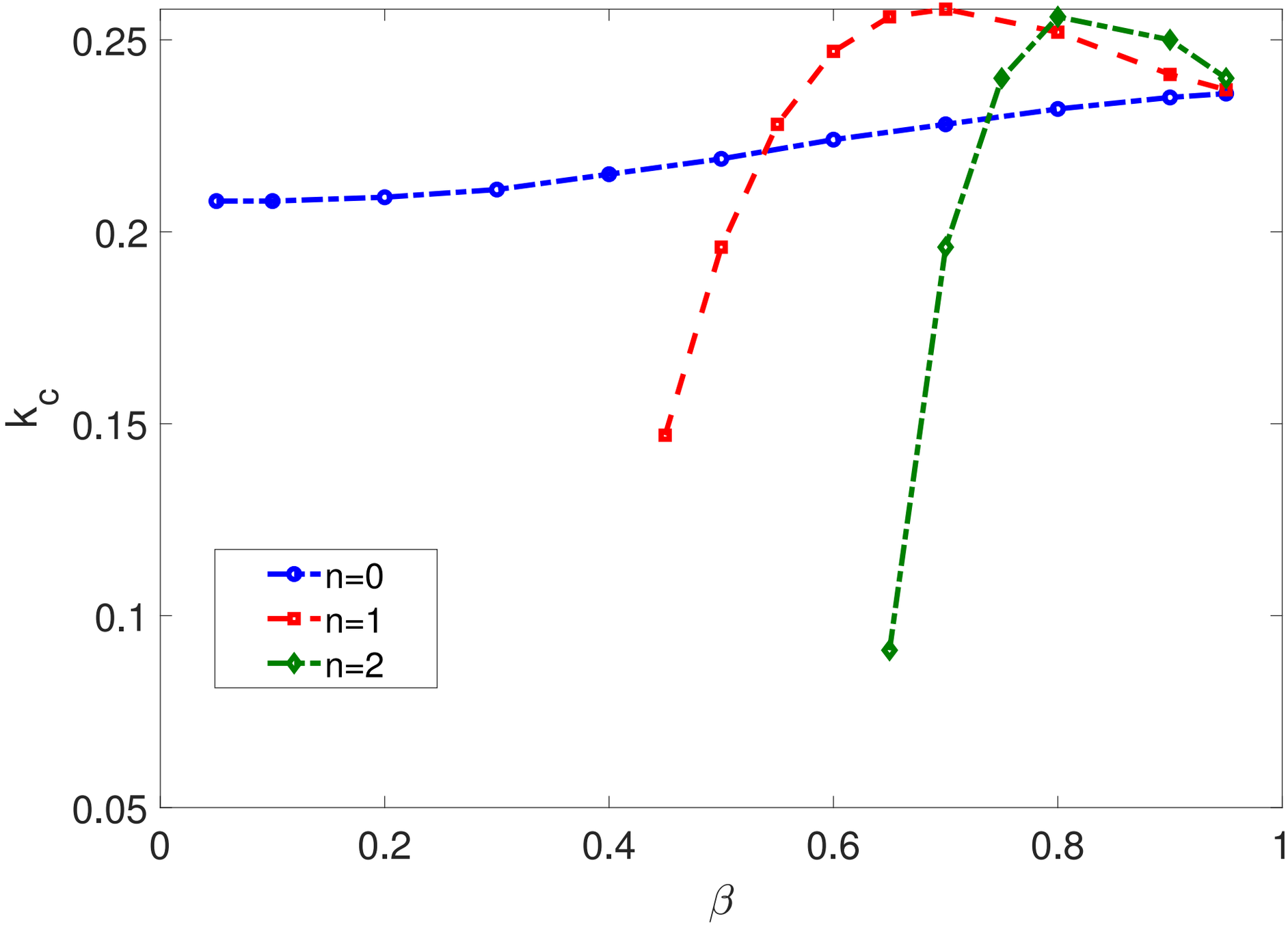
0.25
0.2
0.15
0.1
0.05
k_c
0
0.2
0.4
0.6
0.8
1
β
n=0
n=1
n=2

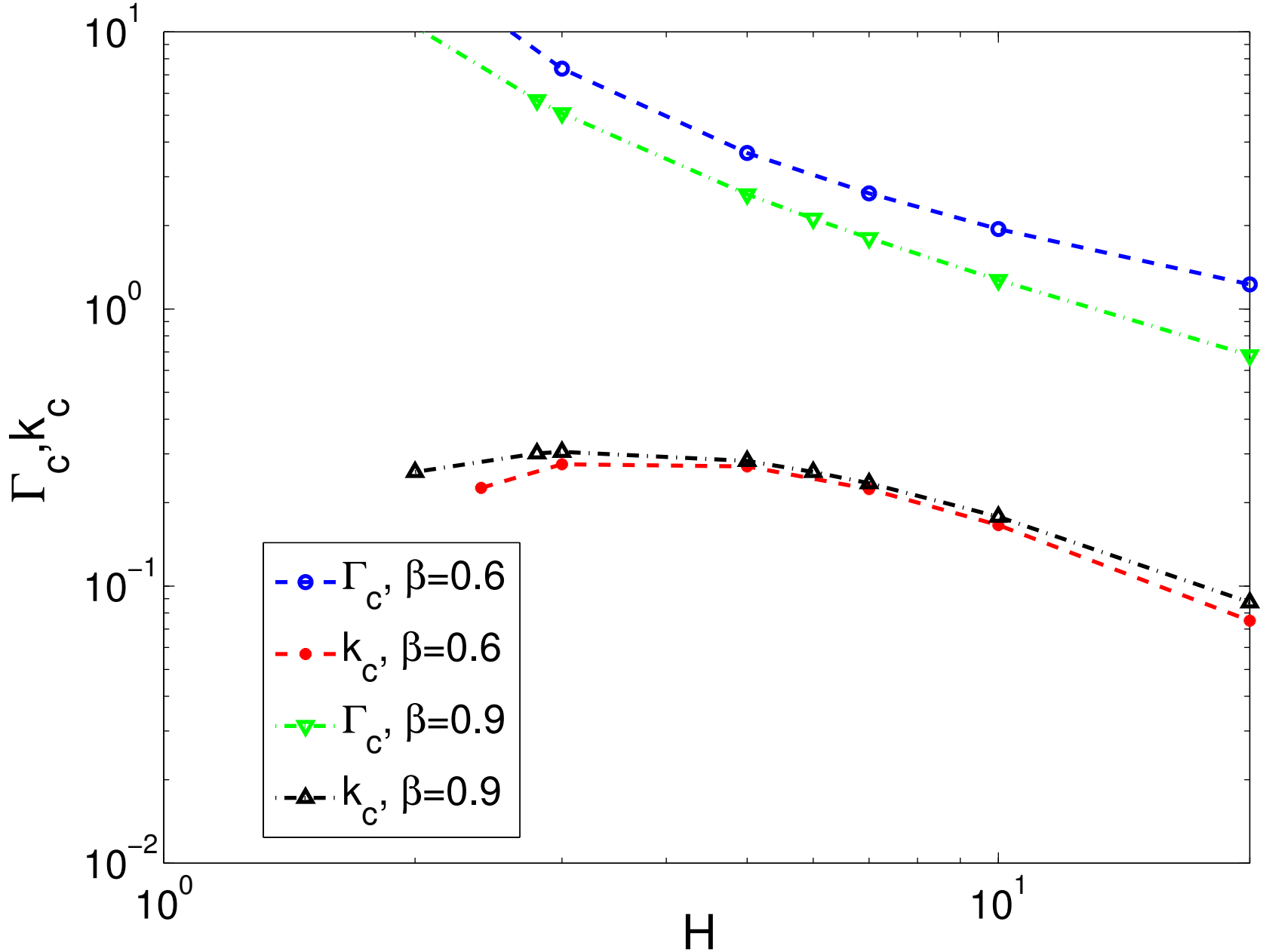
10^1
10^0
10^{-1}
10^{-2}
Γ_c, k_c
10^0
10^1
H
Γ_c, β=0.6
k_c, β=0.6
Γ_c, β=0.9
k_c, β=0.9

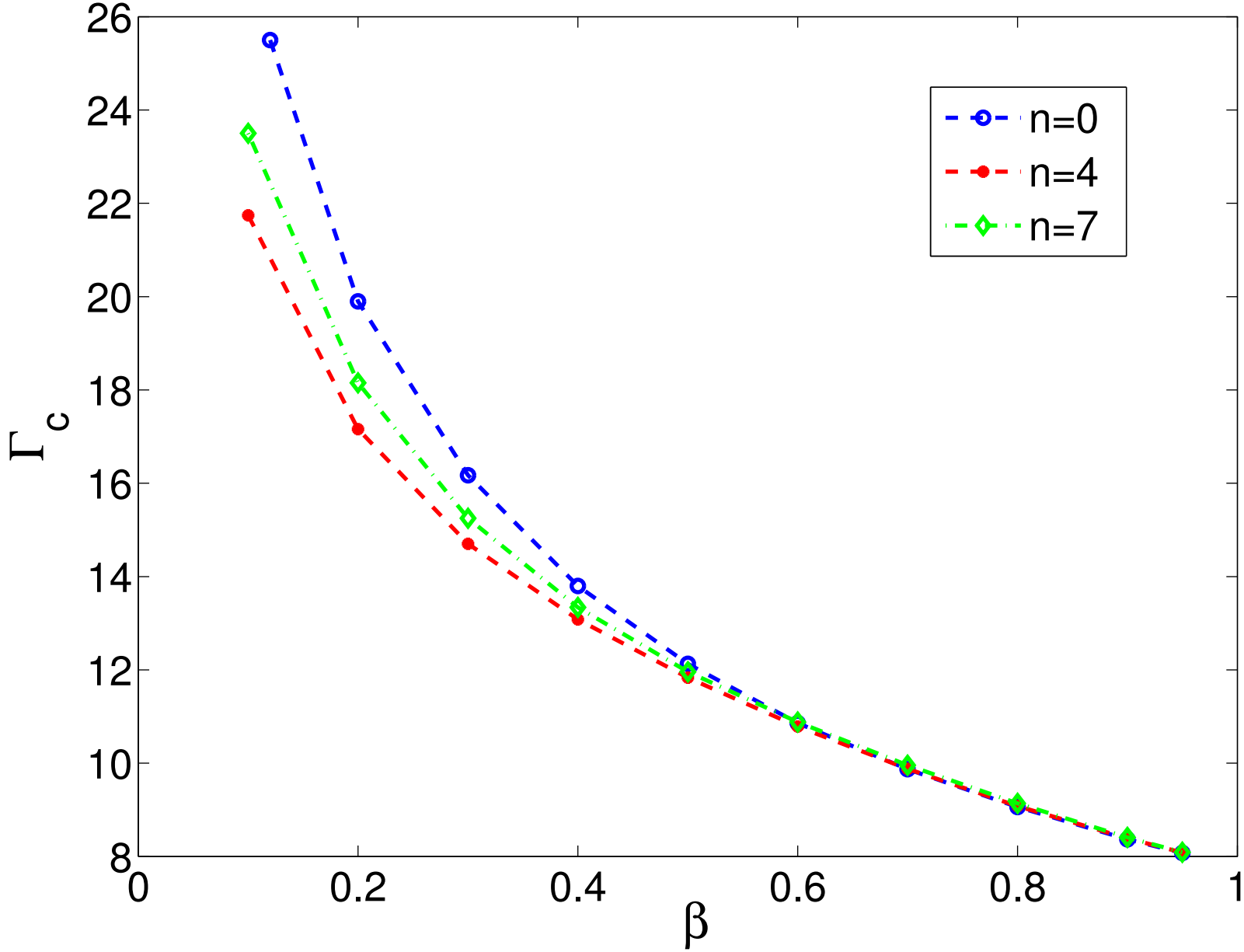
26
24
22
20
18
16
14
12
10
8
0
0.2
0.4
0.6
0.8
1
Γ_c
β
n=0
n=4
n=7

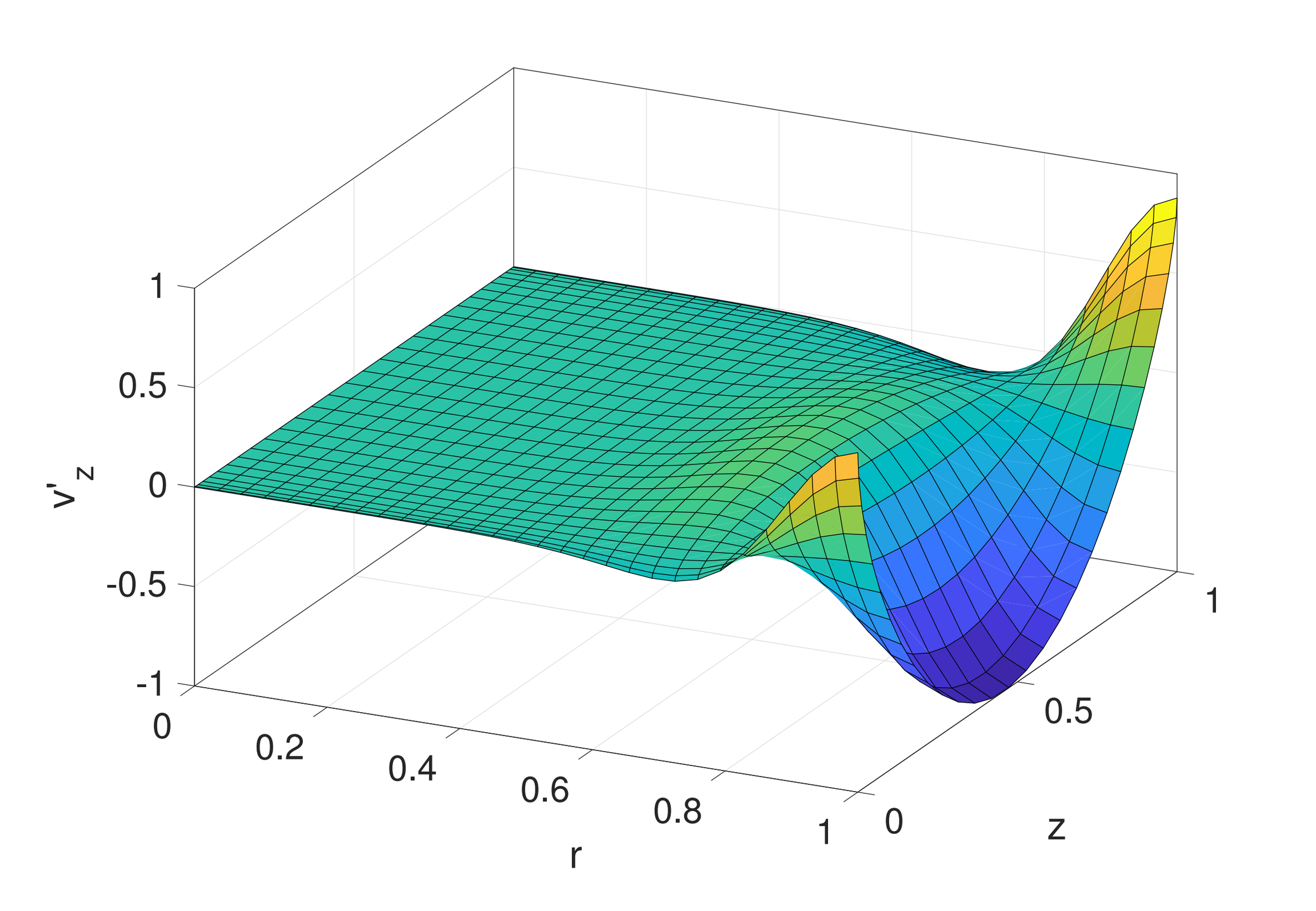
1
0.5
0
-0.5
-1
v'z
0
0.2
0.4
0.6
0.8
1
r
0
0.5
1
z

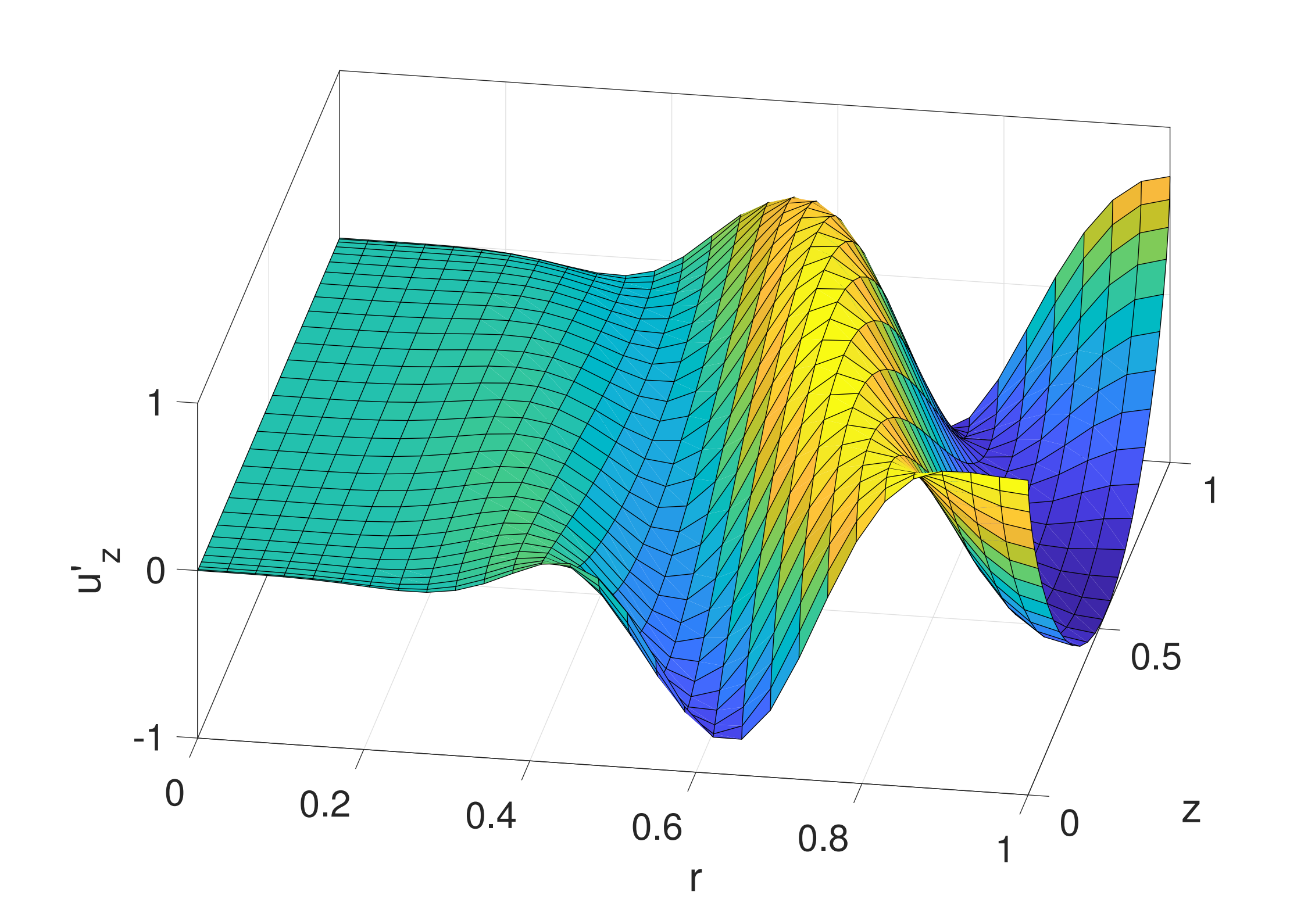
1
0
-1
u'z
0
0.2
0.4
0.6
0.8
1
r
0
0.5
1
z

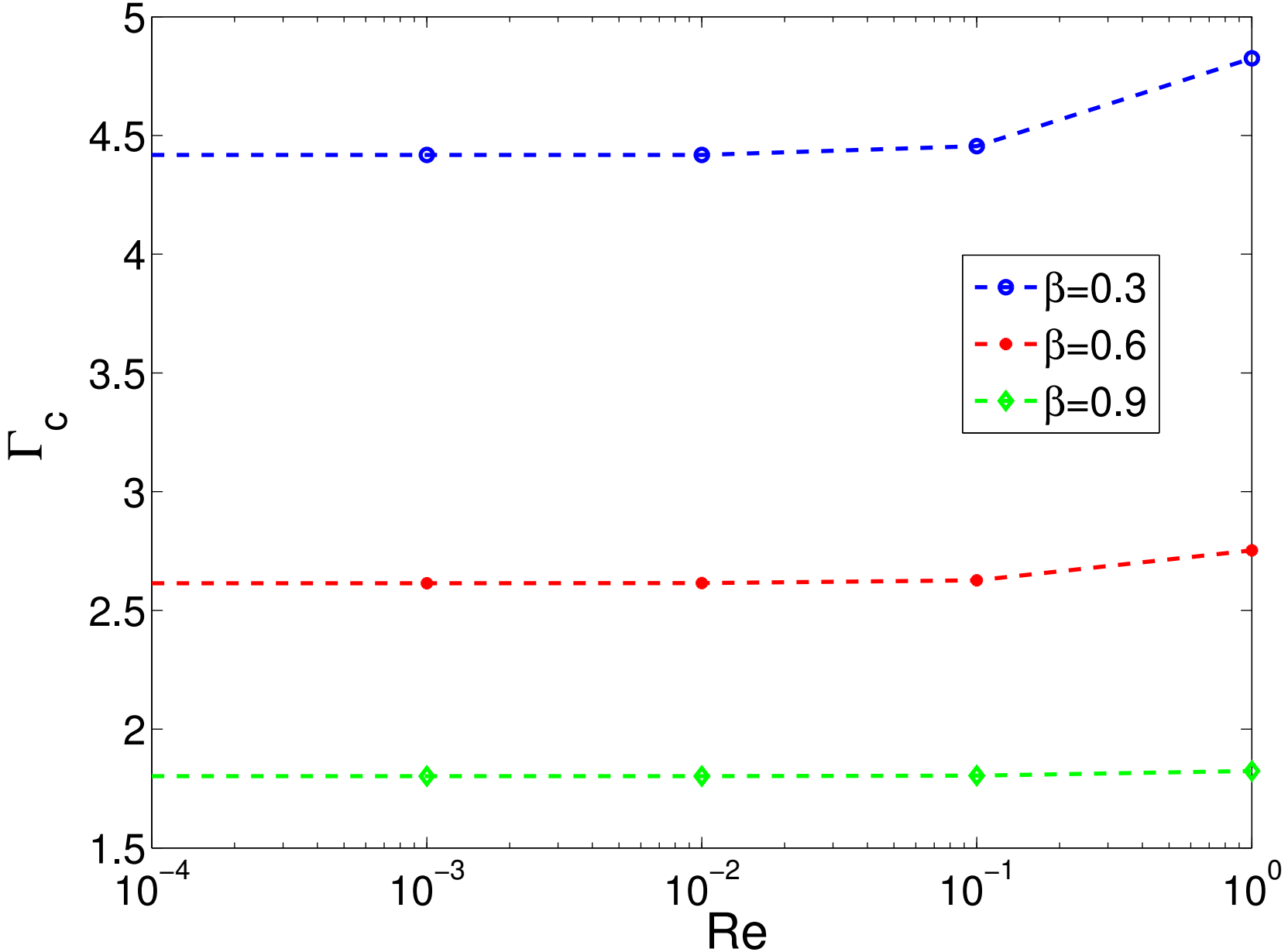
5
4.5
4
3.5
3
2.5
2
1.5
Γ_c
10^{-4}
10^{-3}
10^{-2}
10^{-1}
10^{0}
Re
β=0.3
β=0.6
β=0.9

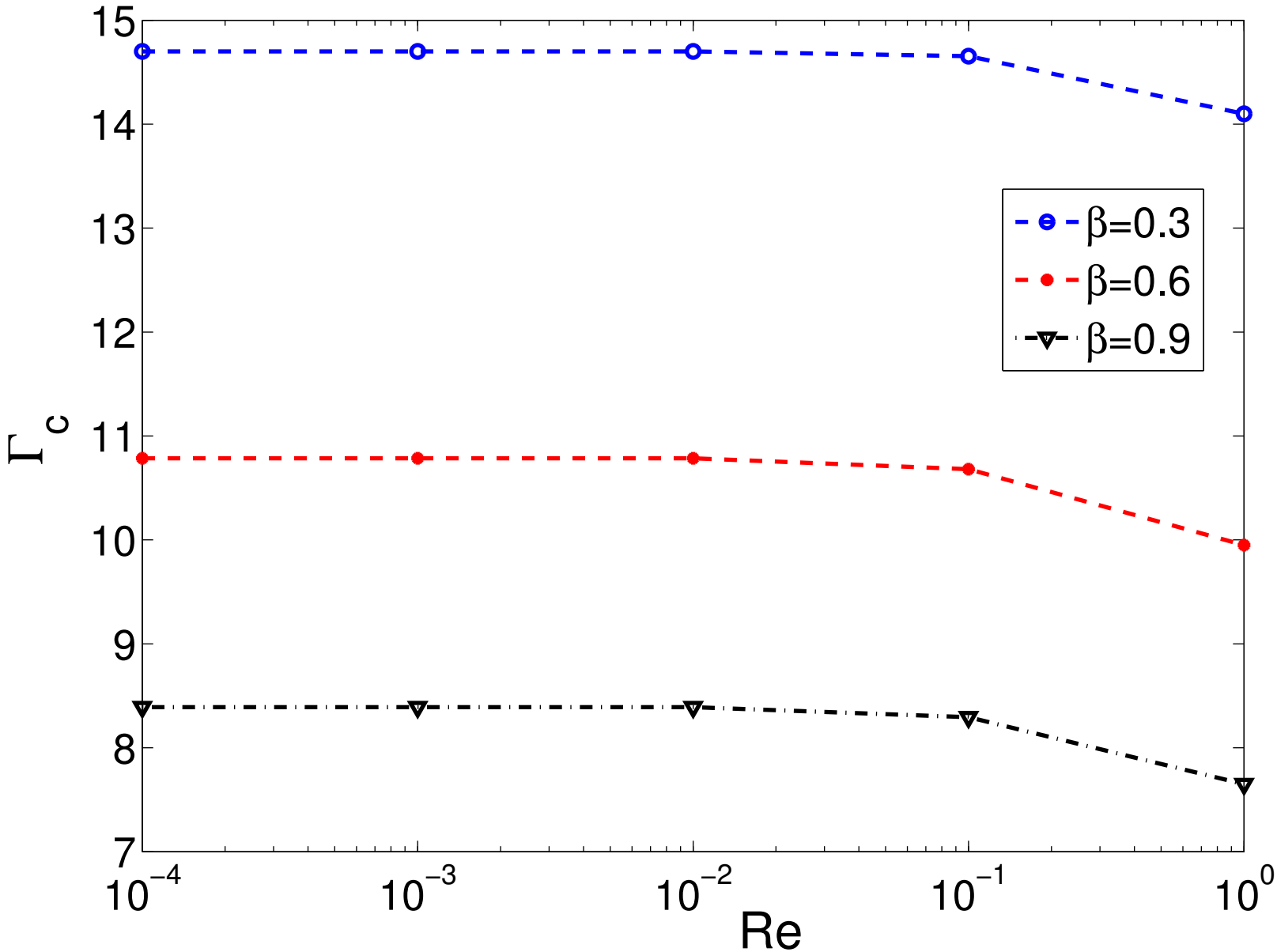
15
14
13
12
11
10
9
8
7
Γ_c
10^{-4}
10^{-3}
10^{-2}
10^{-1}
10^{0}
Re
β=0.3
β=0.6
β=0.9

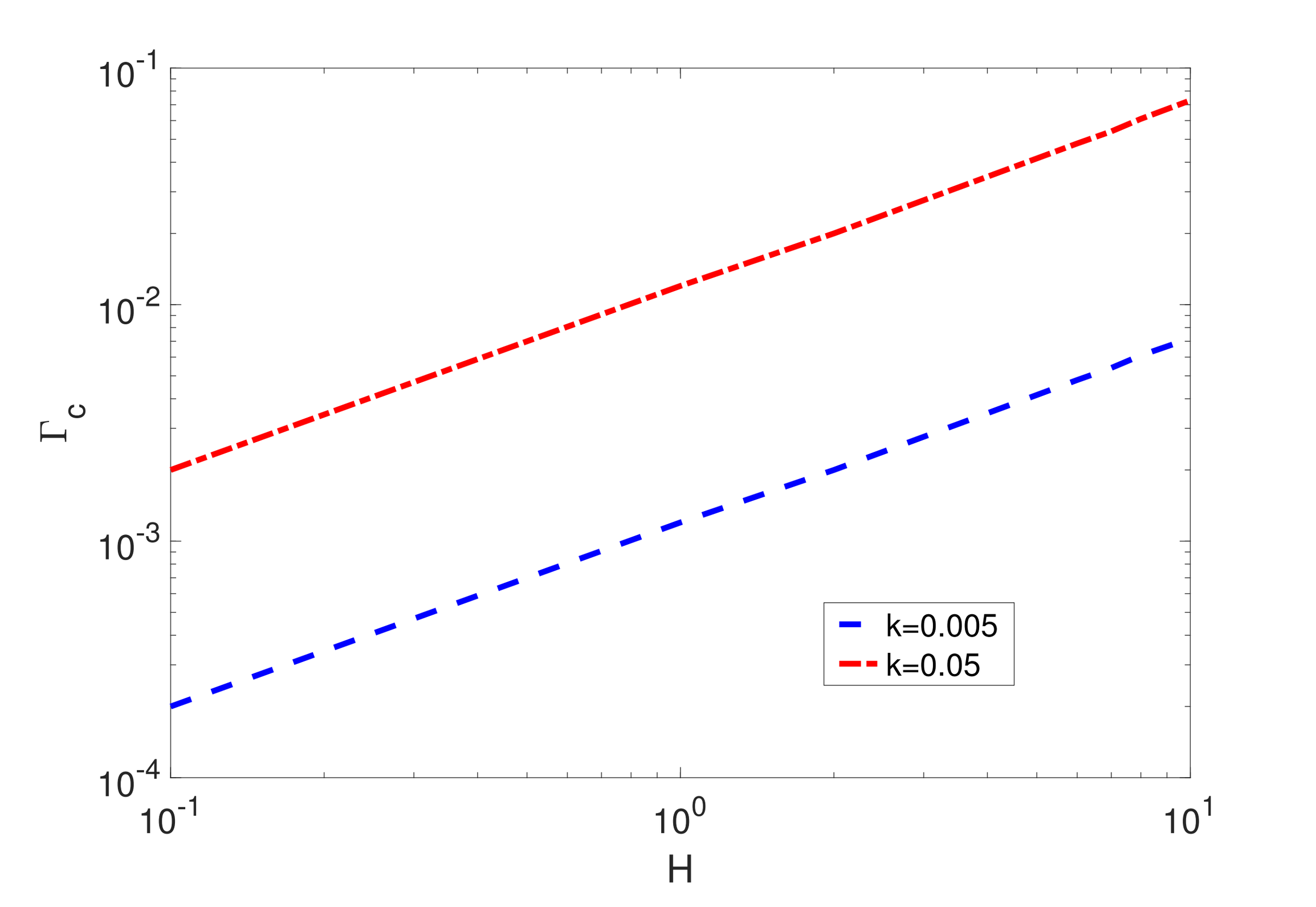
10^{-1}
10^{-2}
10^{-3}
10^{-4}
Γ_c
10^{-1}
10^{0}
10^{1}
H
k=0.005
k=0.05